INFORMATION TO USERS

This material was produced from a microfilm copy of the original document. While the most advanced technological means to photograph and reproduce this document have been used, the quality is heavily dependent upon the quality of the original submitted.

The following explanation of techniques is provided to help you understand markings or patterns which may appear on this reproduction.

1. The sign or "target" for pages apparently lacking from the document photographed is "Missing Page(s)". If it was possible to obtain the missing page(s) or section, they are spliced into the film along with adjacent pages. This may have necessitated cutting thru an image and duplicating adjacent pages to insure you complete continuity.

2. When an image on the film is obliterated with a large round black mark, it is an indication that the photographer suspected that the copy may have moved during exposure and thus cause a blurred image. You will find a good image of the page in the adjacent frame.

3. When a map, drawing or chart, etc., was part of the material being photographed the photographer followed a definite method in "sectioning" the material. It is customary to begin photoing at the upper left hand corner of a large sheet and to continue photoing from left to right in equal sections with a small overlap. If necessary, sectioning is continued again — beginning below the first row and continuing on until complete.

4. The majority of users indicate that the textual content is of greatest value, however, a somewhat higher quality reproduction could be made from "photographs" if essential to the understanding of the dissertation. Silver prints of "photographs" may be ordered at additional charge by writing the Order Department, giving the catalog number, title, author and specific pages you wish reproduced.

5. PLEASE NOTE: Some pages may have indistinct print. Filmed as received.

Xerox University Microfilms
300 North Zeeb Road
Ann Arbor, Michigan 48106

Downloaded from SHAREOK. Persistent Handle URL: https://hdl.handle.net/11244/4050

76-3131

SCOTT, Robert Patrick, 1942-
THE ELECTRICAL BREAKDOWN OF ARGON AND NITROGEN.

The University of Oklahoma, Ph.D., 1975
Physics, fluid and plasma

Xerox University Microfilms, Ann Arbor, Michigan 48106

THIS DISSERTATION HAS BEEN MICROFILMED EXACTLY AS RECEIVED.

THE UNIVERSITY OF OKLAHOMA

GRADUATE COLLEGE

THE ELECTRICAL BREAKDOWN OF ARGON AND NITROGEN

A DISSERTATION

SUBMITTED TO THE GRADUATE FACULTY

in partial fulfillment of the requirements for the

degree of

DOCTOR OF PHILOSOPHY

By

ROBERT PATRICK SCOTT

Norman, Oklahoma

1975

THE ELECTRICAL BREAKDOWN OF ARGON AND NITROGEN

APPROVED BY

Richard S. Fowler

J M Cornfield

S. E. Babb Jr.

R. Kantowski

William N. Huff

Dissertation Committee

DEDICATION

This dissertation is dedicated to my children, Leslie and Marc.

ACKNOWLEDGEMENTS

The author is grateful to many who have contributed their time and effort to the completion of this dissertation. A special note of thanks must go to Dr. R. G. Fowler for his continued advice and assistance throughout the experiment.

The author will be forever indebted to Dr. William C. Paske, who wrote the wave speed computer program, drafted the final drawings for this dissertation and shared his home and friendship with me during this trying period.

Gratitude must be extended to Mr. Gopal Misra and Ms. Denice Thomas for their assistance in the laboratory and in particular to Dr. Roger N. Blais for the original design and construction of the breakdown apparatus.

The experiment could not have been completed without the excellent machine work of Mr. Gene Scott and Mr. Woody Porter or the exceptional glassblowing of Mr. Ron Stermer. The typing of the rough draft was well accomplished by the sleepy-eyed Ms. Virginia Ralls and the outstanding quality of the final draft is a result of the efforts of Ms. Jaquine Littell.

Finally, I wish to express both love and gratitude to my children who gave me the inspiration to carry this work to its completion.

Financial support for the author was furnished by the United States Navy in the form of a Naval Weapons Center Fellowship.

TABLE OF CONTENTS

Page

Acknowledgements iv

LIST OF ILLUSTRATIONS. vi

Chapter

I. INTRODUCTION 1

II. EXPERIMENTAL APPARATUS 5

A. Wave Launching Apparatus 5

The Power Supply 5
The Breakdown Tube 9
The Vacuum System. 14

B. Diagnostics. 17

Wave Speed Diagnostics 18
The Electrostatic Probe. 23

III. DATA ANALYSIS. 32

A. Wave Speed Analysis. 32

B. Determination of Electric Field. 35

C. Experimental Results 46

D. Comparison to Theory 52

IV. CONCLUSIONS AND SPECULATIONS 56

BIBLIOGRAPHY 58

APPENDIX A: TABLES FOR ELECTROSTATIC PROBE CALIBRATION DATA . . 59

APPENDIX B: ELECTRIC FIELD AND WAVE SPEED RAW DATA FOR NITROGEN AND ARGON. 63

APPENDIX C: WAVE SPEED COMPUTER PROGRAM 75

LIST OF ILLUSTRATIONS

Figure		Page
1.	Marx Step Generator	1
2.	Driver Assembly	10
3.	Voltage Divider Circuit	10
4.	The Breakdown Tube	12
5.	The Initiating Electrode	13
6.	The Vacuum System	16
7.	Wave Speed Device	19
8.	RCA 7265 Photomultiplier	22
9.	The Electrostatic Probe	25
10.	Impedance Matching Circuit	27
11.	Electrostatic Probe Oscillograms	30
12.	Wave Speed Sample Data Run	76
13.	Mock-up of Breakdown Tube	36
14.	Probe Voltage Profile Curve for the Breakdown Tube	38
15.	Probe Voltage Profile Curves for the Mock-up Apparatus	39
16.	Probe Voltage versus Applied Voltage for Nitrogen and Argon Antiforce Waves	41
17.	Probe Voltage versus Applied Voltage for Nitrogen and Argon Proforce Waves	42
18.	Voltage Profile Curves Relating the Electric Field to the Applied Voltage	44
19.	Proforce Curves for Nitrogen Gas	47

Figure Page

20. Antiforce Curves for Nitrogen Gas 48

21. Proforce Curves for Nitrogen Gas. 49

22. Antiforce Curves for Argon Gas. 50

THE ELECTRICAL BREAKDOWN OF ARGON AND NITROGEN

CHAPTER I

INTRODUCTION

The process by which a gas changes from an insulating state to a conducting state has been of interest to man since it was first observed in the form of lightning. The first serious investigation was performed by Francis Hauksbee,[1] who observed in 1705 that light flashes were emitted from the evacuated tube over the mercury column of a barometer when the instrument was vibrated. Numerous experiments have since been performed that contributed much to the qualitative understanding of the breakdown process but all attempts to solve Maxwell's equations had failed to produce a quantitative description of the process.

In 1962 Fowler and Paxton[2] presented a preliminary quantitative theory that achieved reasonable agreement with experimental results for precursor waves observed in an electric driven shock tube. The theory was based on a three fluid model of electrons, positive ions and heavy neutrals. Instead of Maxwell's equations, they combined Poisson's equation with the fluid dynamical equations for conservation of mass, momentum and energy of the three components and then sought solutions in which the luminous front was viewed as a shock wave in

the electron fluid.

In 1964 Haberstich[3] performed an innovative study of breakdown waves in helium and argon for both positive and negative applied voltages up to 10 KV and pressures from 0.1 torr to 10.0 torr. In this experiment, he established a well defined ground for the electrostatic field by enclosing the tube within a coaxial metal cylinder. He also made wave speed measurements as a function of both pressure and the wave front potential by using photomultiplier tubes and electrostatic probes. Finally, he measured the electron density of the quasi-neutral region behind the wave front by using microwave interferometry. In spite of these advances there are several objections that prevent the comparison of his results to a quantitative theory. First, his gas purity is in doubt because he only employed a mechanical fore pump to evacuate his system. Second, the accuracy of his wave speeds are dubious since he only used the time base of a dual beam oscilloscope for single events. Finally, he never calibrated his electrostatic probe for the electric field.

In 1967, George Shelton[4] proposed a one dimensional quantitative theory for breakdown waves based on the three fluid model of Paxton and Fowler. He found a rigorous solution to the fluid dynamical equations for the case of a wave traveling in the direction an external field would accelerate an electron. This wave corresponds to the negative ionizing wave of Haberstich and was designated by Shelton as a <u>proforce wave</u>. The case where wave propagation and electron acceleration oppose each other was given the designation of <u>antiforce wave</u>. In 1974, Everett Sanmann[5] completed the one dimensional theory by solving the

fluid dynamical equations for the case of antiforce waves.

In 1971, Roger Blais[6] sought experimental results in a form suitable for comparison with Shelton's theory. He performed a study of helium for both proforce and antiforce waves to applied voltages of 40 KV and pressures from 0.3 torr to 30.0 torr. In contrast to Haberstich, he made wave speed measurements as a function of pressure and the electric field of the wave front. The statistical wave speed technique he employed was far superior to the single event measurements of Haberstich but instead of using electrostatic probes for the electric field he extrapolated his velocities to the driving electrode where the applied voltage was known. He then employed a theoretical expression to relate this voltage to a value for the electric field at the wave front. Where Haberstich had measured the electron density of the quasineutral region with microwaves, Blais attempted to measure the electron temperature and density of the wave front using the optical technique described by Latimer, Mills and Day.[7] This method also measured the quasi-neutral region because the response time of his photomultiplier was not fast enough to detect the electrons in the narrow sheath region of the front.

The experimental results of both Blais and Haberstich are somewhat dubious and unsuitable for a valid test of the Shelton and Sanmann theories. The purpose of the experiment described in this dissertation was to combine the best features of both experiments and attempt to achieve results that could be used to check the validity of the theories. The electrostatic probe of Haberstich was used to measure the electric field at the wave's front and the statistical wave

speed technique of Blais was used to measure the velocities.

CHAPTER II

EXPERIMENTAL APPARATUS

A. Wave Launching Apparatus

The wave launching apparatus was basically the same as that employed by Blais and consisted of three main parts; the power supply, the breakdown tube and the vacuum system. However, a few changes were made to improve the apparatus. The major changes were in the power supply and the vacuum system, so, these two sections will be discussed in detail. The breakdown tube was thoroughly described by Blais and only the modifications will be pointed out here.

The Power Supply

The power supply used in the previous work of Blais was capable of attaining a maximum voltage of 40 KV with a rise time of less than 20 nanoseconds. The power supply to be discussed in this section was specifically designed to deliver voltages as high as 100 KV with a rise time less than 20 nanoseconds. The purpose of the higher voltage was to determine if the breakdown wave had an upper limit in velocity.

The simplest known method to achieve high voltages with fast rise times is with a Marx Step Generator. The Marx generator is basically a voltage multiplier circuit consisting of N capacitors charged

in parallel to a voltage V_0 and then connected in series to give a resultant voltage of NV_0. The fast rise time is accomplished by using spark gaps between the capacitor stages to perform the task of switching from parallel to series. Using this technique the output voltage will approximate a step voltage of amplitude NV_0. In practice, the step voltage is applied to a resistance R that will drain the voltage off the capacitors at an exponential rate where the time required for one e-folding of the voltage is $t = RC$ and is called the decay constant of the voltage signal.

The Marx Step Generator used in this experiment is shown in Figure 1. Actually, two separate generators were required to achieve the desired voltage and decay constants, but the description that follows will apply to both. The power supply consisted of a control panel that contained a charge and discharge switch, a variac and an ammeter; the power supply proper which contained a Plastic Capacitor 50 KV Power Pak, an isolation transformer, three capacitors and their associated charging resistors, the switching spark gaps and a high voltage solemoid relay; the driver assembly which contained the actuating spark gap, the load resistors and the voltage monitor circuit. The control panel was located external to the power supply proper which was enclosed in a shielded room to prevent the spark gap radiation from interfering with the diagnostics. In operation, sixty cycle A.C. from the control panel entered the power supply through a lowpass filter to a Sola isolation transformer and was then applied to the primary of the 50 KV Power Pak. The Power Pak is a sealed unit containing a step-up transformer, two silicon rectifiers and two high voltage capacitors

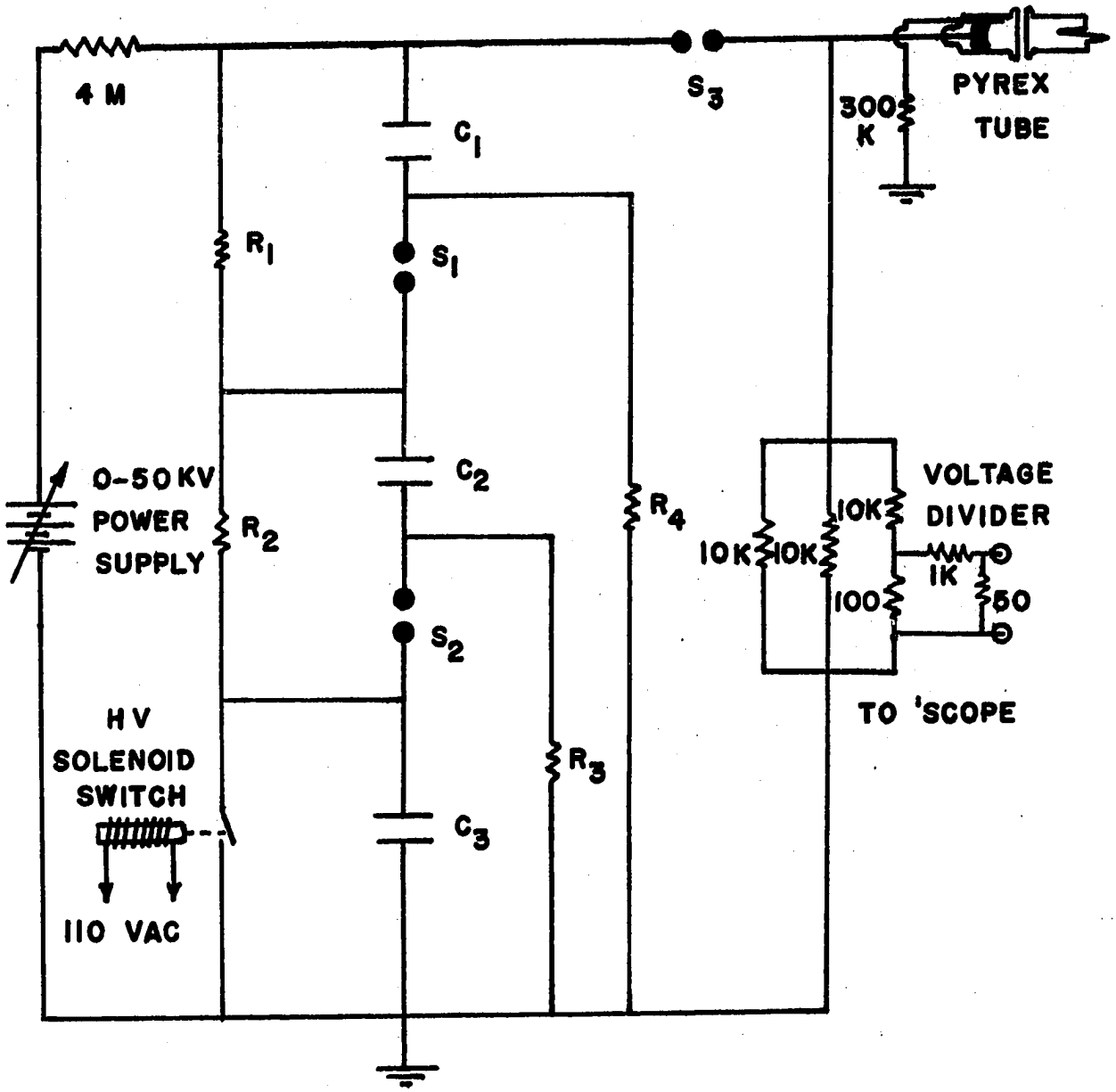

Component	Range of Voltage 0-30KV	40-100KV
R_1, R_2, R_3	10 K	300 K
R_4	30K	900 K
C_1, C_2, C_3	1.0 μf	0.025μf

FIGURE 1. MARX STEP GENERATOR.

all connected as a voltage doubler circuit. The output voltage is rectified with a very small ripple factor and is proportional to the input voltage. The input voltage was controlled by means of the variac and ammeter on the remote control panel. Varying the input voltage from 0 to 110 V A.C. yields output voltages from 0 to 50 KV D.C. This output voltage was applied through a 4 M resistor to the three capacitor stages and their associated charging resistors. The values of the charging resistors are given in the table of Figure 1 but are not required for the purpose of this discussion. It is sufficient to state at this point that the values are such that the capacitors will all charge at the same rate, which is proportional to the voltage of the Power Pak. When the capacitors are all charged to the value V_0 the spark gap S_2 will breakdown and connect capacitors C_2 and C_3 in series resulting in a voltage of $2V_0$ being felt across S_1 which in turn breaks down, applying $3V_0$ across S_3. At this point a step voltage of amplitude $3V_0$ has been developed. Next, the actuator spark gap S_3 breaks down and switches the step voltage to the three 10K load resistors and the breakdown tube electrode. The load resistors develop the voltage being applied to the tube and cause the exponential decay of the step voltage. The capacitors continue to charge and discharge automatically, as long as the "Charge" switch of the control panel is turned on. When a data run is completed the charge switch is turned off and the discharge switch turned on which activates the high voltage solenoid switch connected across C_3 and any residual voltage left on the capacitors will drain off to ground. The repetition frequency and decay time of the 0-30 KV generator were 4 PPM (pulses per minute) and 1.5

milliseconds, respectively and 1 PPS (pulse per second) and 30 microseconds, respectively, for the 40-100 KV generator.

Figure 2 illustrates the structure of the driver assembly. As mentioned earlier, the driver assembly contains the actuating spark gap, the three 10K load resistors and the voltage monitoring circuit. The spark gap itself was constructed from two aluminum spheres with inlaid gold on the active surface between them and a mechanical control system. The sphere on the breakdown tube side was fixed into position, but the sphere on the power supply side could be moved by a screw so that the gap separation could be varied. The resistors were symmetrically mounted in the form of a cone about the axis of the breakdown tube. These low inductance carbon resistors served the double function of providing mechanical support for one side of the actuating spark gap and of prividing the electrical path to ground so that the actuating spark gap would discharge with stability and reliability. In addition, one of the resistors was made part of a 2320 to 1 resistive voltage divider circuit. The voltage divider circuit illustrated in Figure 3 was built into a cylindrical aluminum block to shield the resistors from spark gap radiation. The spacing between the aluminum block and the resistors had to be large to minimize the stray capacitance which tends to increase the measured rise time. The design used in this voltage divider circuit resulted in measured rise times less than 20 nanoseconds for voltages up to 80 KV.

The Breakdown Tube

The breakdown tube section was the heart of the experiment where the initiation and propagation of the wave occurs. The breakdown tube

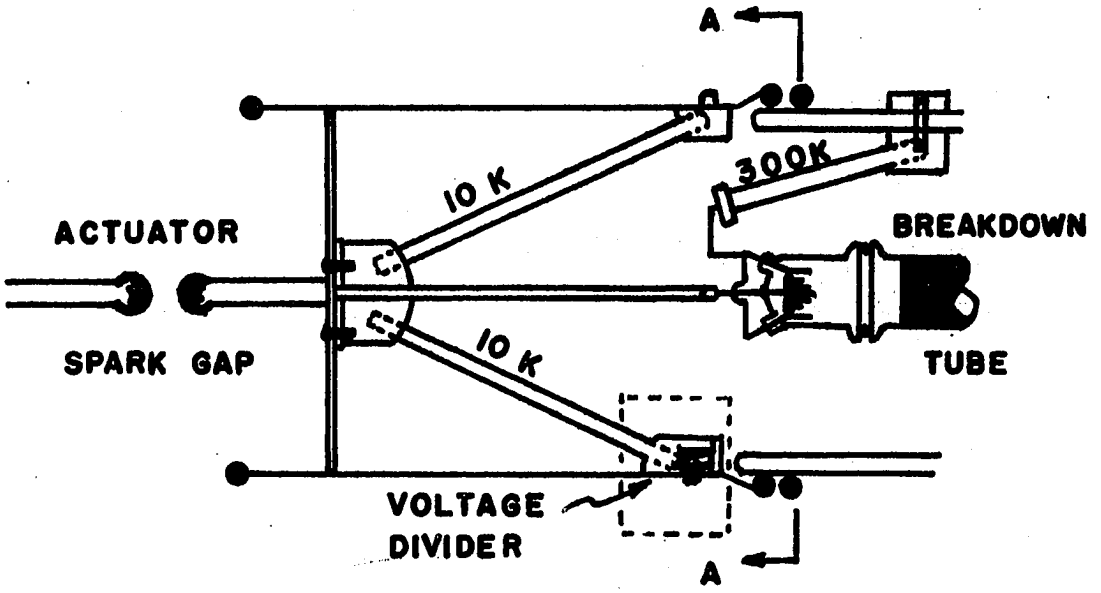

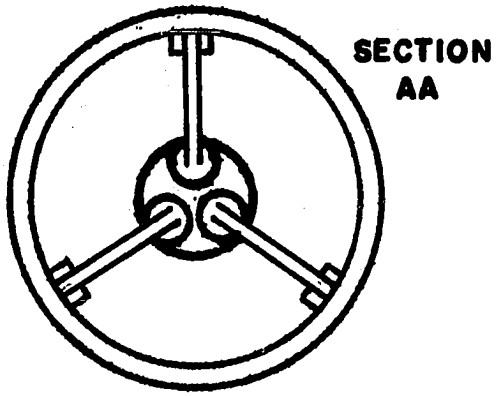

FIGURE 2. DRIVER ASSEMBLY.

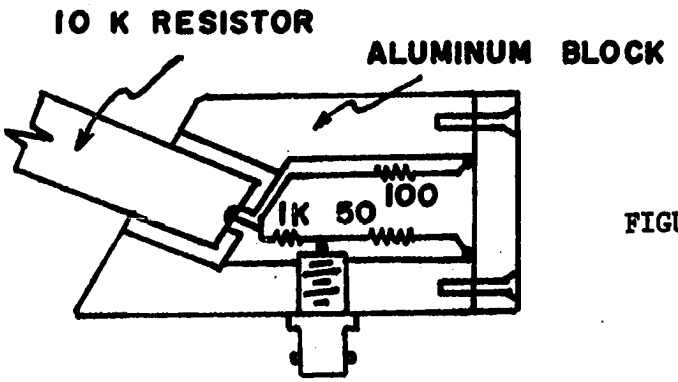

FIGURE 3. VOLTAGE DIVIDER CIRCUIT.

consisted of a long straight Pyrex tube filled with gas to be tested, a removable electrode to initiate the wave, an electrostatic ground array to provide a simple known geometry for the electric field and to shield the wave from stray fields, a series of light pipes to locate permanent viewports on the tube, a rail and cart system to firmly support the optical diagnostics and a wooden table to support the whole affair. The breakdown tube illustrated in Figure 4 was basically the same as described by Blais except for a few modifications that will be pointed out here.

The Blais discharge tube was a 7.3 meter long straight piece of Pyrex 7740 pipe line tubing with a five centimeter inner diameter and a five-eighths centimeter wall thickness. The initiating electrode and vacuum system were permanently attached to opposite ends of the tube. This design did not allow for any future changes in the initiating electrode, the size of the discharge tube or the vacuum system. In order to make the tube compatible with present and future design modifications, O-ring seal joints were attached to both ends of the tube. The end joints were made from five centimeter inner diameter and five-eights wall thickness Pyrex 7740 pipe line tubing, the same as the discharge tube.

Wave initiation requires the presence of electrons in the vicinity of the electrode. Blais experimented with several electrode designs that exploited field emission and settled on a shape that resembles a florist's frog with sharp pointed spines. The longest spines were in the middle so that their full effect on field emission would not be diminished by those farther from the central axis, as would have been

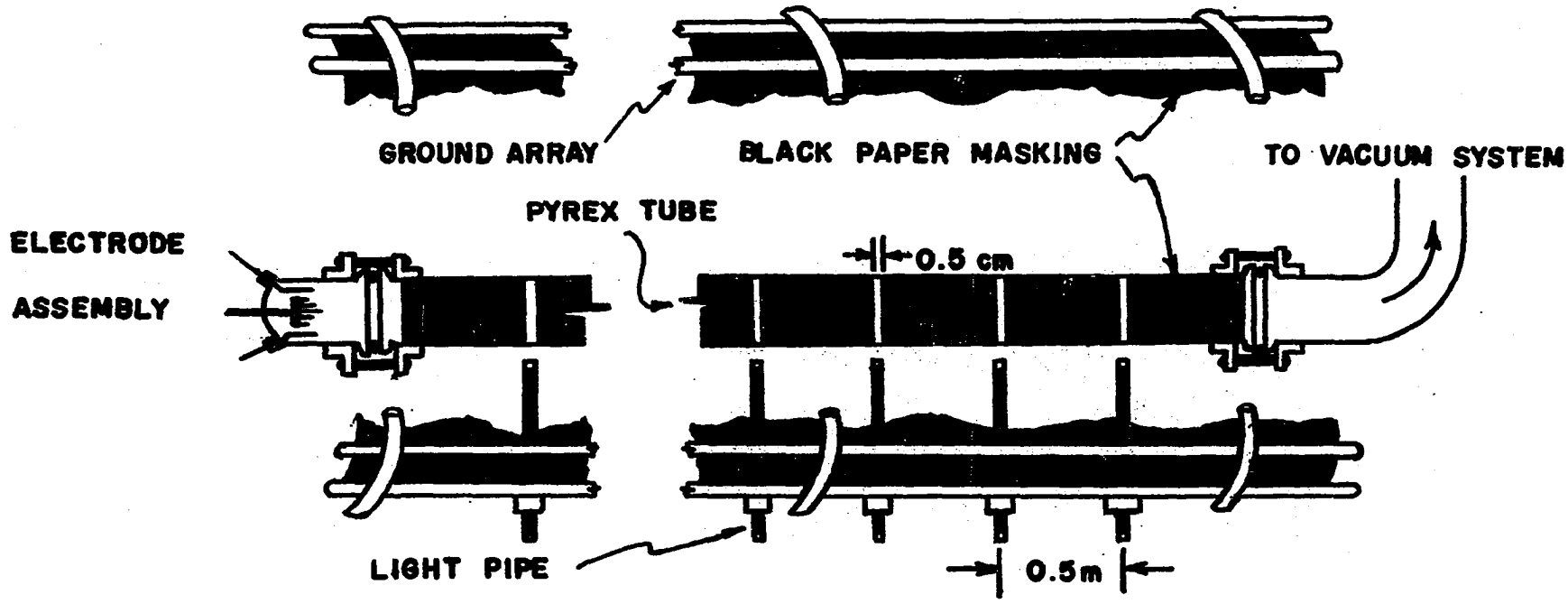

FIGURE 4. THE BREAKDOWN TUBE.

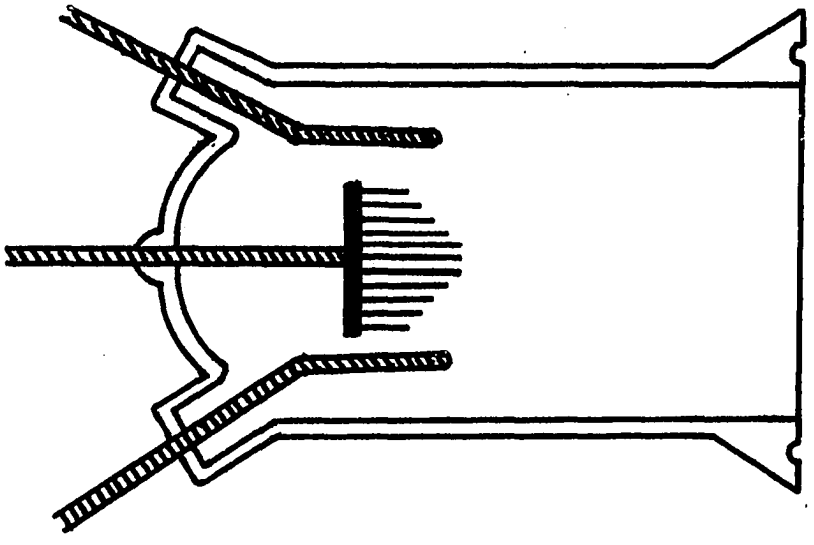

FIGURE 5. THE INITIATING ELECTRODE.

the case with a flat faced electrode. An improvement on this device is shown in Figure 5 and a detailed description follows. The electrode end was constructed from a short piece of Pyrex 7740 tubing identical to the discharge tube. The three electrodes were sealed into one end by means of Wolfram seals. The central electrode was the florist's frog with sharp pointed spines designed by Blais. In addition, two stainless steel pointed prongs were inserted parallel to the central electrode. A 300K resistor was connected to these electrodes and to ground. This gave rise to a small glow discharge when the voltage was applied to the central electrode, which provided additional electrons for wave initiation. The end result was that wave initiation occurred close to the leading edge of the voltage signal with greater reliability. The opposite end was an O-ring seal joint that easily made up with the discharge tube using nylon clamps to minimize field distortion.

The bleeder electrode at the far end of the old discharge tube was removed and made an integral part of the vacuum system to be discussed in the next section. Also, plexiglass spacers were inserted between the two halves of the electrostatic ground array to prevent the propagation of electromagnetic waves. The metal rail system for the optical diagnostics was replaced with wood to prevent the Lecher line behavior that had interfered with the photomultiplier operation previously.

The Vacuum System

The vacuum system designed by Blais was fabricated entirely

from glass with no O-ring seals. It also connected to much smaller inner diameter tubing between the breakdown tube and the vacuum pumps. The lack of O-ring seals hindered any future modification of design as pointed out in the previous section. Also, the small tubing restricted the pumping action and created a margin of uncertainty in gas purity of the breakdown tube. Both of these problems were eliminated by installing sections of five centimeter I.D. tubing with O-ring seals from the breakdown tube all the way back to the vacuum pumps. Figure 6 illustrates the O-ring tubing and the rest of the vacuum system.

The main components of the system were a Duo-Seal model 1402 mechanical fore pump, an NRC type HSA two inch air cooled diffusion pump, a Matheson regulator, a Temescal HY-Vac needle valve and a McLeod gauge. The Temescal valve was made of brass and served as the bleeder electrode for the discharge tube. One end of a 30K resistor was connected to the valve and the other end was attached to the electrostatic ground array. When the luminous wave front reached the valve a glow discharge was formed in the tube which drained the charge off the walls of the discharge tube. The NRC 531 thermocouple gauge and the NRC Bayard-Alpert 563 ionization gauge used by Blais were eliminated from the system and the McLeod gauge was the only standard employed for all pressure readings. The ultimate system pressure was well below 0.1 micron and perhaps as much as an order of magnitude lower. The total volume of the system was thirteen liters, nine of which were the tube itself.

The procedure for filling the tube with gas began with pumping

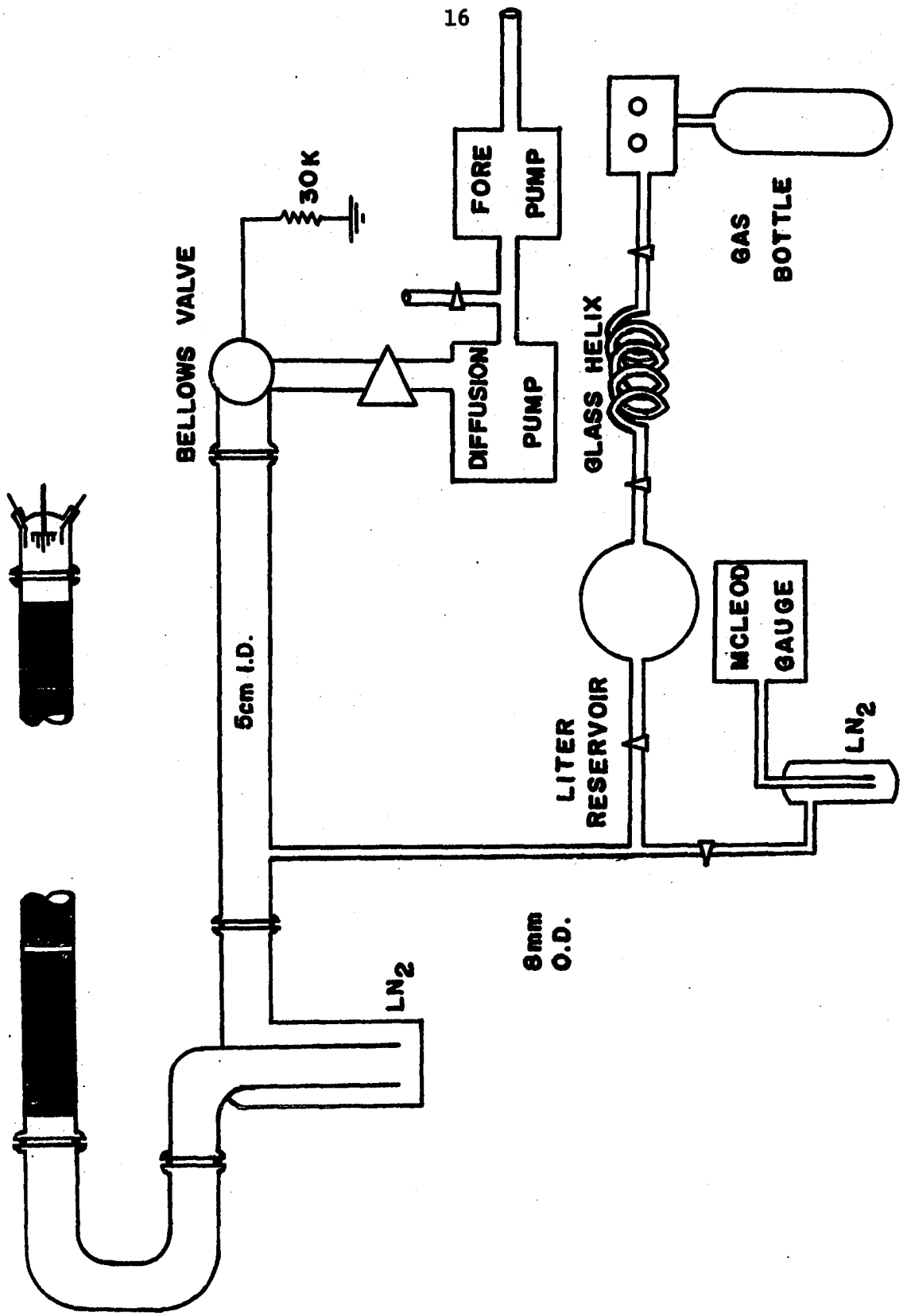

FIGURE 6. THE VACUUM SYSTEM.

the tube down to ultimate pressure as read on the most sensitive McLeod gauge scale. Then the system was allowed to pump for at least one additional hour. Then the Temescal valve between the system and the pumps was closed and the pressure was read at intervals to determine if any leaks were present. In the absence of any leaks, Matheson research grade Argon or Nitrogen containing no more than 5 PPM impurities was injected via the regulator which had been pumped out to the bottle valve. This gas filled a one liter reservoir to just over one atmosphere of pressure. The entire system was then flushed out with clean gas and the reservoir was refilled with fresh gas. Finally, using a manometer, for approximate pressure readings, clean gas was allowed to leak into the system until the desired pressure was attained. Next, the bottom end of the liquid nitrogen cold trap on the breakdown tube end of the vacuum system was chilled. A few minutes later when the impurities had frozen out on the bottom of the trap, the rest of the trap was immersed in liquid nitrogen. The two stage process ensures that as the nitrogen level drops by evaporation the worst impurities will remain in the trap. Then, after a few moments to equilibrate, the tube pressure was accurately measured by the McLeod gauge.

B. Diagnostics

An experiment can not be performed without the aid of instruments to measure the phenomenon being studied. The luminous wave of this experiment propagates with a velocity that is dependent on the electric field at the front and the neutral gas pressure ahead of the

wave. Gas pressures were measured using the calibrated McLeod gauge. This section describes the diagnostics used to measure the velocity and the electric field of the front.

Wave Speed Diagnostics

Wave speeds were measured by a method similar to that employed by Blais, a method which offers high absolute time resolution, statistical compilation of the results of many events and the elimination of the need for carefully matched photomultipliers. This method used two photomultiplier tubes stationed at half centimeter slotted viewports distributed at quarter meter intervals along the tube. The PM outputs were coupled through timed cables to the start and stop inputs of a time to pulse height converter. The TPHC output pulse was voltage analyzed by a multichannel analyzer which could assemble and store the results of a statistically significant number of events. Data on time intervals between observations ports were then displayed on an oscilloscope or printed out on a teletype.

In this experiment the multichannel analyzer was eliminated and the TPHC output voltage was coupled directly to a Tektronix 555 dual beam oscilloscope. The amplitude of the voltage signal was directly proportional to the time difference between the start and stop inputs and could be calibrated against known delay lines. A visual average of the voltage amplitude for a significant number of events was found to give results equivalent to the MCA method and was less time consuming. A block diagram of the wave speed device is shown in Figure 7. The experimental technique was to leave the start PM at a

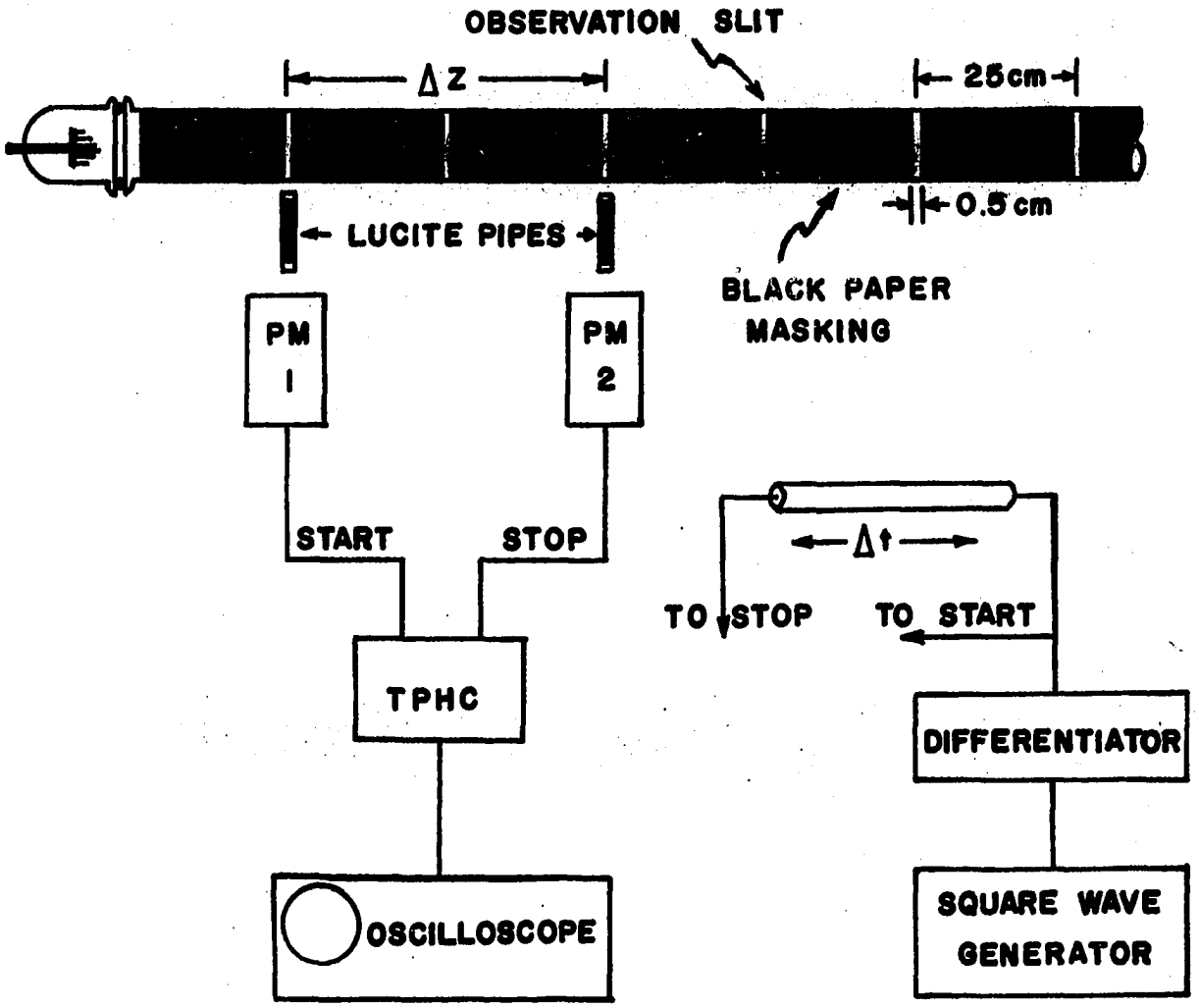

FIGURE 7. WAVE SPEED DEVICE.

fixed position on the tube and progressively move the stop PM to successive ports accumulating distance versus time data which were later converted to velocity versus distance.

Wave Speed System Components

Photomultipliers.

Two different types of phototubes were utilized in measuring the time of flight of the waves. The PM with the shortest transit time was used for the start signal which resulted in a builtin delay between the two tubes. This avoided the possibility of a difference in rise time on the PMs coupled with a fast wave and a short distance between the two observation ports causing the stop pulse to arrive at its TPHC input before the start pulse could get to its input. Exact knowledge of the path lengths of the two PMs was avoided by subtracting the first data point from those that followed. Blais compensated for attenuation in light intensity as the wave progresses down the tube by increasing the applied voltage on the stop PM. This results in a decrease in the transit time and rise time of the PM which would invalidate the measured time of flight. Fortunately, it was seldom necessary and most of his data was taken with an applied voltage of 800V. To avoid any such occurrence in the present work both PMs were operated with an applied voltage of 1500V which was sufficient to cause saturation of the light pulse.

The start PM was an RCA 7746 mounted at the lucite light pipe located one meter from the driving electrode and was described in detail by Blais. The stop PM was an RCA 7265 mounted in an aluminum

housing with the circuit shown in Figure 8. The 7265 is a fourteen stage head on, in line, spherical faceplate tube with a maximum spectral response at 4200 ± 500 Å. It has a multialkali (Potassium-Sodium-Cesium-Antimony) photocathode with S-20 spectral response, Copper-Beryllium dynodes and a Corning #0080 lime glass window. The maximum cathode to anode voltage rating is 3000V, the anode pulse rise time is 2.7 nanoseconds and the luminous sensitivity at the anode is 65 amps per lumen. The can in which the PM was mounted enclosed it completely except for a small hole 3/4 inch in diameter in the center of the faceplate. This hole exactly matched the size of the light pipe it mated with. The signal of both PMs was coupled out by double shielded coax cable with intrinsic delay time of about 40 nanoseconds. The additional shielding was necessary to prevent RF pickup from the power supply at voltages above 40 KV. The PMs were mounted on a cart and rail assembly to facilitate positioning along the tube.

Time to Pulse Height Converter.

The TPHC was a standard ORTEC model 437 which was described in detail by Blais and only the points that directly apply to this experiment will be repeated in this section. The output voltage was a bipolar pulse, as shown below, whose amplitudes were directly proportional to the time difference between the start and stop inputs. It was calibrated against delay lines known to roughly one nanosecond. There was a combination of 15 selectable time scales ranging from 50 ns to 80 μs full scale. The delay lines used to calibrate the TPHC were 50 ohm RG-58/U cable and are described in the 1970 dissertation of Gary E. Copeland.[8]

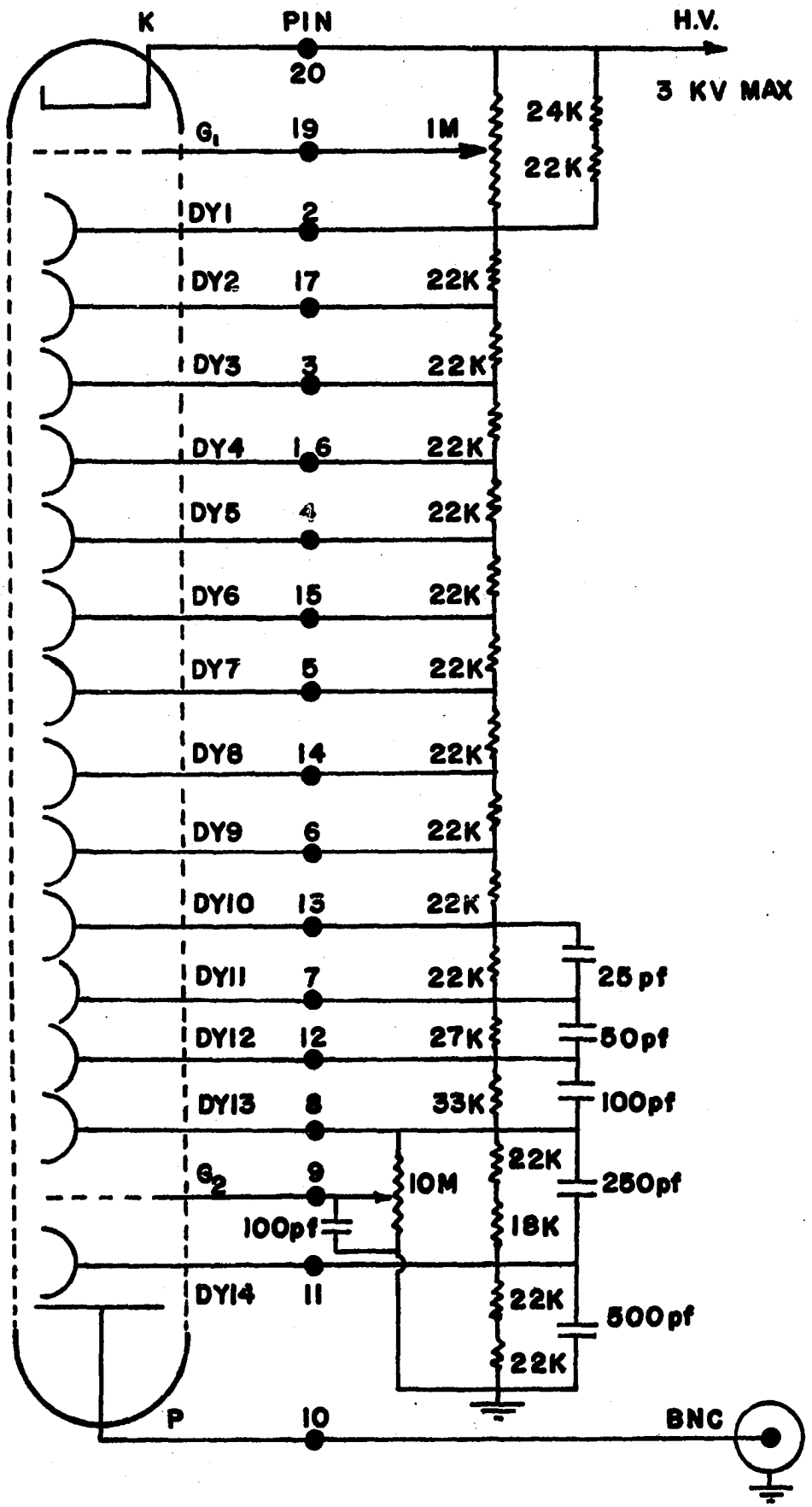

FIGURE 8. RCA 7265 PHOTOMULTIPLIER.

The calibration data for the first nine time scales were taken and put into a computer program that will be discussed in the chapter on data analysis. The experimental procedure was to record the TPHC time scale used and the amplitude of the positive pulse for each station of a data run. This data was then inserted into the computer program which computed the desired velocities.

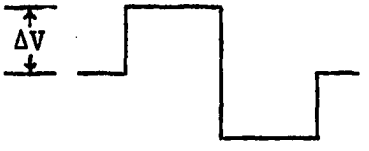

Bi-Polar Pulse

The Electrostatic Probe

The most significant distinction between the work of Blais and the present experiment was the determination of the electric field at the wave front. The method employed by Blais was based on a theoretical calculation of S.E. Babb, Jr.,[9] who solved Poisson's equation for the boundary conditions of a half infinite pair of concentric cylinders. The calculation resulted in a value for the electric field along the tube axis of

$$E = \frac{0.507}{a} V = 0.203\ V$$

Where a = the radius of the plasma column = 2.5 cm

V = the potential at the front of the plasma column

Blais used this result to compute a single value of electric field at the electrode where the wave potential was equal to the applied potential. He then found an empirical expression for velocity versus distance

which was extrapolated back to the electrode to get an initial value of velocity that could be associated with the value of electric field. This method resulted in one data point for each data run at a fixed applied voltage.

In this experiment the electric field of the wave front was measured at each position along the tube with the aid of an electrostatic probe. The E.S. probe was not unique to this experiment but was previously used in the work of Haberstich. Haberstich managed to couple his probe signal through a 125 ohm coax cable to an oscilloscope with a 125 ohm input impedance without the aid of any impedance matching circuitry. His probe apparently had sufficient capacitance to accomplish this without any noticeable differentiation or distortion of the signal. Since the rise time of the probe signal is determined by the wave velocity, the amplitude of a differentiated signal would be proportional to the velocity of the wave front. In the present work, coupling the probe signal directly through a 50 ohm coax cable to an oscilloscope terminated in 50 ohm resulted in signal differentiation. Increasing the value of the termination to eliminate the differentiation resulted in signal distortion. Numerous attempts to achieve an impedance match using linear matching techniques also proved unsuccessful. Finally, the writer had to resort to non-linear matching techniques which resulted in total success.

The electrostatic probe itself (Figure 9) consisted of a short section of 50 ohm RG 58/U coax inserted into a brass sleeve for rigidity. The brass sleeve was permanently attached at one end to a shielded black box which contained the impedance matching circuit. The sleeve

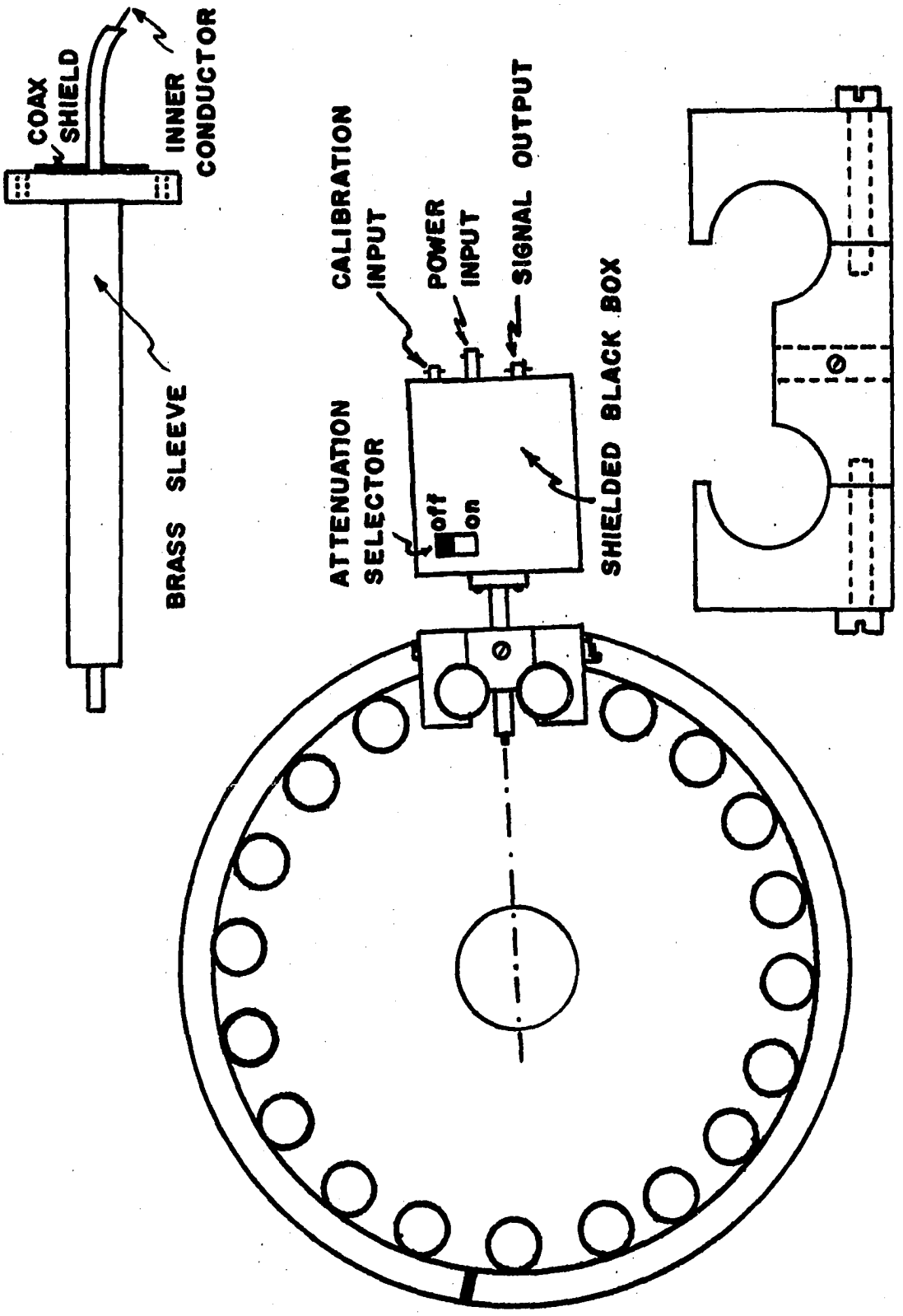

FIGURE 9. THE ELECTROSTATIC PROBE.

fit smoothly inside an aluminum clamping device that held the probe securely between the bars of the breakdown tube. A screw on the side of the clamping device held the probe firmly in position once the penetration depth had been selected. A short piece of aluminum angle was fastened to the bottom of the clamping device that braced against the next lower bar which aligned the probe with the axis of the breakdown tube. The braided shield of the coax was pressed between the sleeve mounting plate and the wall of the black box. The inner conductor of the probe was soldered to the center contact of the Attenuation Selector switch mounted on the side of the black box. Input power to the black box was facilitated by means of a Tri-Ax UHF bulkhead connector that had two inner conductors. The Circuit Test Input and Signal output connectors were both UG-290A/U BNC connectors. All the data was taken with a probe penetration depth of 1.5 centimeters.

The impedance matching circuit is shown schematically in Figure 10 and a detailed description is given below. The power requirements for the circuit were ±15 VDC with a nominal power consumption of 300 milli-watts. The power was supplied by two SORENSON model ORS15-2 power supplies, each capable of providing 3.0 amperes at ±15 VDC and was coupled to the E.S. probe with double shielded Tri-Ax coaxial cable. The input of the matching circuit could be selected for zero or 2:1 attenuation by the two position Attenuation Selector switch labeled S_1. In the OFF position the probe signal is connected directly to the 22 megohm resistor on the gates of a pair of complementary field effect transistors. In the ON position a voltage divider is formed

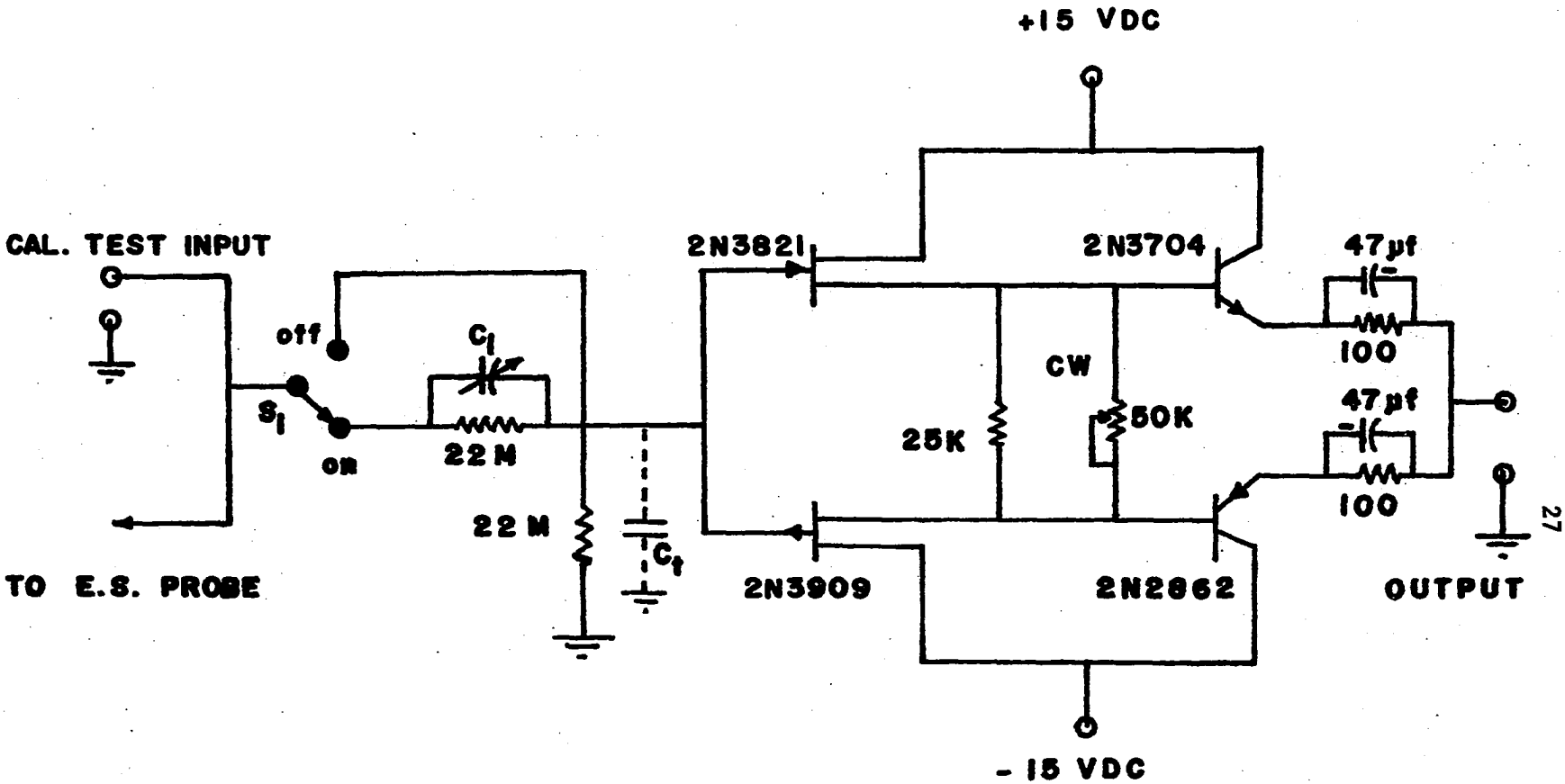

FIGURE 10. IMPEDANCE MATCHING CIRCUIT.

by the two 22 megohm resistors between S_1 and the gates of the two FETs. The variable capacitor C_1 across the first resistor is used in conjunction with the input capacitance of the FETs for frequency compensation of the input signal. When C_1 is properly tuned the voltage divider circuit becomes a 2:1 attenuator for all frequencies of the input signal. From the gates of the two FETs the signal will follow different paths depending upon its polarity. The 2N3821 FET and the 2N3704 transistor form an emitter follower circuit for negative input signals. The 50K ohm potentiometer across the 25K ohm carbon resistor between the bases of the two output transistors is necessary to provide a proper balance between the two separate circuits. The 100 ohm resistors in the emitters of the output transistors are used to limit the current in the collectors. The 47 μf electrolytic capacitors across these two resistors are a short circuit to the input signal and pass it on to the output load without any attenuation. The output signal is coupled by double shielded 50 ohm RG-58/U coax cable to a 50 ohm termination on the oscilloscope.

The parallel emitter follower circuits were balanced by the following technique. A CENCO audio oscillator was used to supply a 1.0 volt peak to peak, 5 KHz sine wave to the zero attenuation input of the matching circuit. The output signal was observed on a Tektronix 555 oscilloscope. With the 50K ohm potentiometer in the full counter-clockwise position, waveform a) (below) was displayed on the scope. Slowly rotating the potentiometer clockwise the output signal began to approach the shape of the pure sine wave, shown in waveform b) below. The circuit is properly balanced when a pure sine wave is just attained.

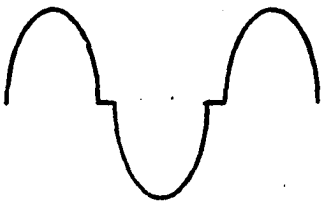

a) Unbalanced

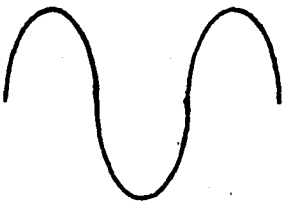

b) Balanced

After the circuit has been balanced the compensating capacitor C_1 can be adjusted. This was accomplished using a DATA PULSE model 100A pulse generator. The generator is capable of providing both positive and negative pulses with amplitudes adjustable from 0.5 to 10 volts and rise times less than 5 nanoseconds when operated into a 50 ohm load. The pulse width is continuously variable from 35 nanoseconds to 10 seconds in seven decade ranges with a 100:1 multiplier. The repetition rate is continuously variable from 0.1 hertz to 10 megahertz in eight decade ranges. The CAL TEST input was connected to one side of a BNC Tee connector and the other side was connected to the positive or negative pulse output of the signal generator. The center connector of the Tee was then connected to a 50 ohm termination on the lower beam of the Tektronix 555 oscilloscope. The SIGNAL output was connected to a 50 ohm termination on the upper beam of the scope. The positive and negative pulses of the signal generator were then adjusted for 2.0 volts amplitude, 0.1 millisecond pulse width and a pulse repetition rate of 1.0 KHz. The compensating capacitor C_1 was then adjusted for the output pulse that most accurately resembled both the positive and negative input pulses. Oscillograms of the positive input and output pulses of the imepdance matching circuit in the unattenuated mode are shown in Figure 11. The rise time of the input pulse (measured between

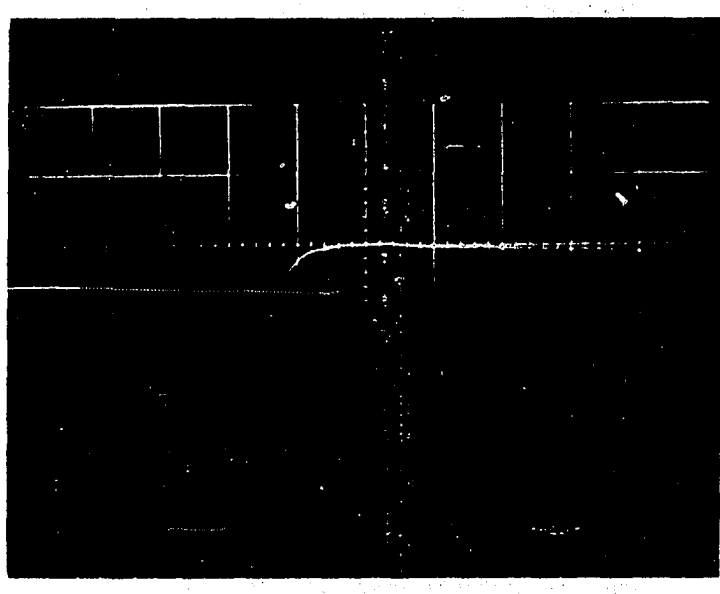

(a) Leading edge of the positive input pulse
vertical: 0.5 v/cm
horizontal: 20 ns/cm

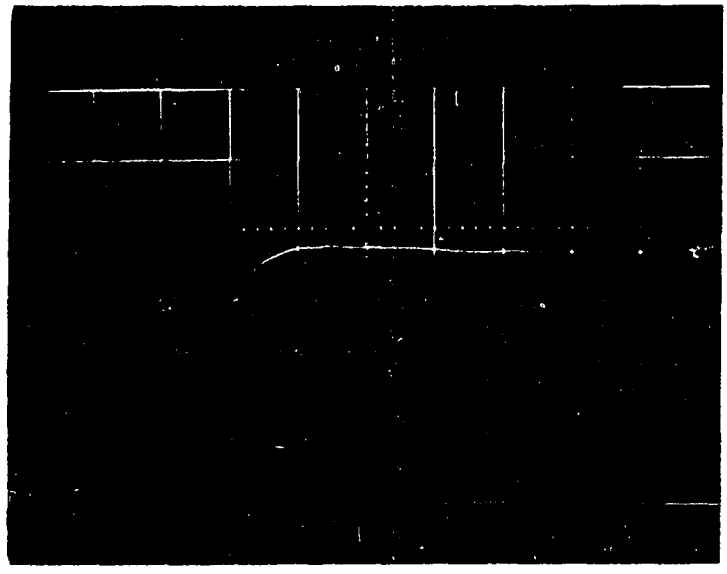

(b) Leading edge of the output pulse
vertical: 0.5 v/cm
horizontal: 20 ns/cm

FIGURE 11. ELECTROSTATIC PROBE OSCILLOGRAMS.

the 10% and 90% points) was 12 nanoseconds and the rise time of the output pulse was 16 nanoseconds. With the 2.0 volt input pulse the emitter follower efficiency was 92.5%. The output pulse had a 10% droop in amplitude between the leading and trailing edge due to insufficient capacitance for the 0.1 millisecond pulse width. This was not important because the leading edge was the only region of interest. The characteristics of the circuit for a negative 2.0 volt input pulse were about the same as stated above, except for the output rise time which was 20 nanoseconds.

It should be stated at this point that all the diagnostic handling equipment (except for the electrostatic probe and the photomultipliers) were enclosed in a Faraday Cage. The Faraday Cage used was a Shielding Inc. stock #8201-706079 Electromagnetic Shielding Encloser fabricated for electronic test purposes. The Cage consisted of two layers of copper screening, a radiation tight door and bulkhead feed through connectors for diagnostic access. The electrostatic probe and photomultipliers were coupled to their associated power supplies and data handling equipment via the feed through connectors. The Faraday Cage in conjunction with the double shielded coaxial cables on the probe and PM outputs served to reduce the possibility of radiative pickup from the power supply spark gaps.

CHAPTER III

DATA ANALYSIS

A. Wave Speed Analysis

As mentioned in the previous chapter, the wave speed data was recorded as a series of voltage pulse heights that are proportional to the time interval required for the wave to travel from a start trigger located 1.0 m from the electrode to a stop trigger (z-1.0) meters farther down the tube. This data was then put into a computer program which calculated the corresponding velocities for the (z-1.0) distance intervals. The formulation of the contents of the computer program is the subject of the following discussion.

Blais previously demonstrated that the wave velocity has an exponential dependence on the distance z along the tube. Based on this knowledge, he then proceeded to derive an expression for the instantaneous velocity at z. Assuming the time interval t_2-t_1 corresponds to the distance interval z_2-z_1 and the functional dependence of velocity with z as

$$v = v_0 e^{-\beta z} \tag{1}$$

Blais derived a correction factor for changing $\Delta z/\Delta t$ into dz/dt. The final result was

$$v(z_1) = \frac{L}{t_2-t_1} \tag{2}$$

where the effective length L was given by

$$L = \frac{1}{\beta} (e^{\beta \Delta z} - 1) \tag{3}$$

Blais used graphical techniques to determine β which were long and tedious. In the present work, a theoretical expression for β in terms of the known information was sought, in order that the computer could do the tedious work. With the start trigger located at z_0 and assuming the form of eq. 1, we have

$$v = v_0 \, e^{-\beta (z - z_0)} \tag{4}$$

where v_0 is the instantaneous velocity at $z=z_0$ and $t=t_0$. This can be rewritten as

$$\frac{dz}{dt} = v_0 \, e^{-\beta (z - z_0)} \tag{5}$$

Separating variables and integrating yields

$$e^{\beta (z - z_0)} = 1 + \beta v_0 (t - t_0) \tag{6}$$

Now, if we let

$$z = z + \Delta z$$

$$t = t + \Delta t$$

then substituting into eq. 6 gives

$$e^{\beta (z + \Delta z - z_0)} = 1 + \beta v_0 (t + \Delta t - t_0) \tag{7}$$

Subtracting eq. 6 from eq. 7 yields

$$e^{\beta (z - z_0)} \cdot (e^{\beta \Delta z} - 1) = \beta v_0 \Delta t \tag{8}$$

Finally, substituting the right side of eq. 6 for the first term on the left side of eq. 8 and rearranging yields

$$\Delta t = \left(\frac{1}{\beta v_0} - t_0\right) \cdot (e^{\beta \Delta z} - 1) + (e^{\beta \Delta z} - 1) t \tag{9}$$

which is the form of a straight line given by

$$\Delta t = mt + b$$

where

$$m = e^{\beta \Delta z} - 1$$

$$b = \left(\frac{1}{\beta v_0} - t_0\right) \cdot (e^{\beta \Delta z} - 1)$$

The expression for the slope m can be rearranged to give the desired expression for β as,

$$\beta = \frac{\ln(1+m)}{\Delta z} . \qquad (10)$$

In this experiment Δz is the distance interval between successive time of flight measurements and was held fixed at 50 cm.

Using the equations derived above, it is now possible to formulate a computer program that can assimilate the raw data into the instantaneous velocities at each position z along the tube. The computer program consisted of: coded calibration curves for the TPHC, which converted the voltage pulse heights into raw times; normalization of the raw times by subtracting the first time interval from successive intervals; formation of the delta times by subtracting the preceding normalized time from the following time; a linear regression of the delta times versus the normalized times; calculation of β from equation 10 and the slope of the linear regression plot; calculation of the effective length from eq. 3 and the calculated value of β; and the calculation and printing of the velocities at each z for eq. 2 and 4 and the necessary print statements. The complete program is given in Appendix C and a sample data run is illustrated.

B. Determination of Electric Field

The electric field of the wave front was measured using the electrostatic probe described in Chapter II. The probe actually measures the potential of the charge concentration created by the ionizing wave front. Furthermore, the electric field of interest is in the z direction along the axis of the tube but the probe views the radial component of the field from the side of the breakdown tube. Therefore, it was necessary to determine an experimental relationship between the probe voltage and the electric field at the front of the wave. This wasaaccomplished with the aid of a mock-up version of the breakdown tube. The mock-up constructed to facilitate the calibration ofthe electrostatic probe is illustrated in Figure 13 and a detailed description is given below. The apparatus consisted of a coaxial ground array, a 1.5 meter long Pyrex tube with a 5 cm inner diameter, and two wooden end pieces to support the assembly. The materials of construction and the geometrical dimensions, except for the length, are the same as the breakdown tube. A 300K low inductance carbon resistor was connected between the ground array and a falt faced cylindrical conductor inserted halfway into the Pyrex tube. A high voltage power supply was coupled to the apparatus through an actuating spark gap attached to the cylindrical conductor. The power supply consisted of a 0.5 μf capacitor that was charged through a 5M resistor by the 50KV Power Pak described earlier. The power supply voltage was adjusted by the spark gap and measured by a Shallcross model 760 D.C. Kilovoltmeter connected across the capacitor.

The first step in the calibration procedure was to properly

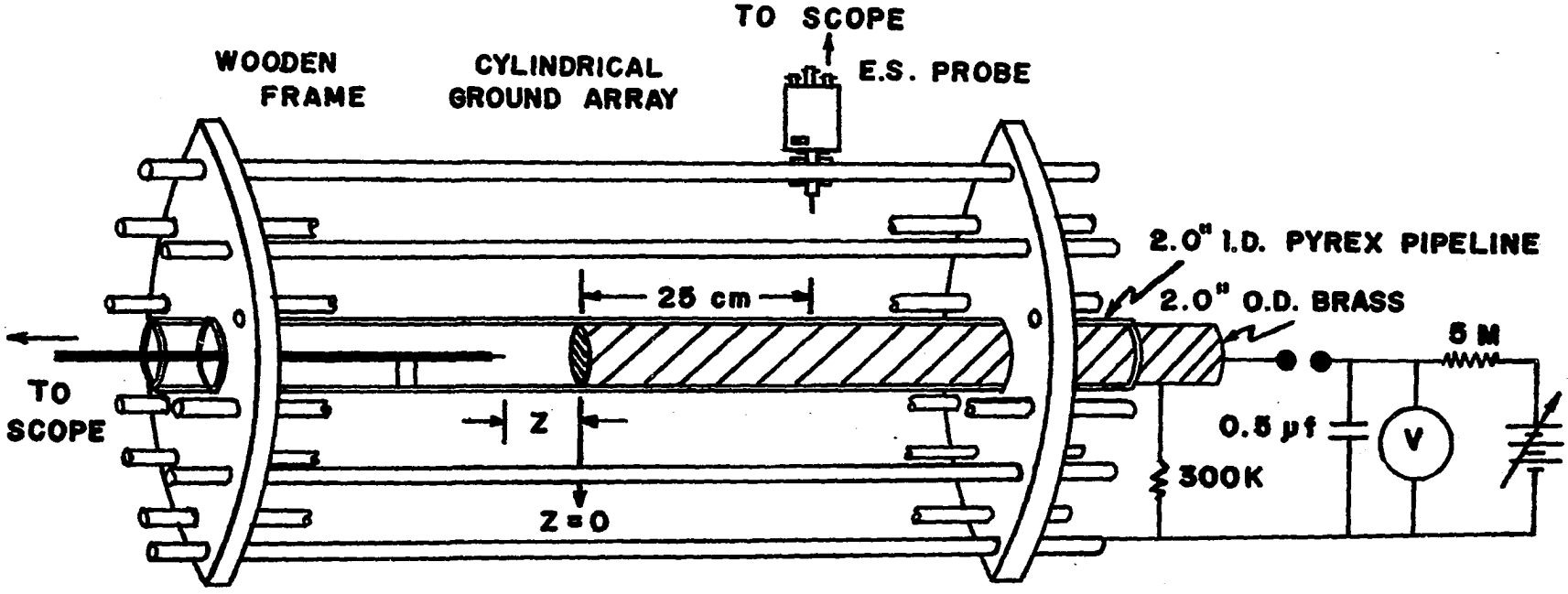

FIGURE 13. MOCK-UP OF BREAKDOWN TUBE.

position the electrostatic probe on the side of the breakdown tube and the mock-up apparatus. The axial positions were determined from the electrostatic probe voltage profile curves discussed below. The breakdown tube voltage profile of Figure 14 was made with an applied voltage of +20 KV on nitrogen gas at a pressure of 1.6 torr. The probe was moved along the side of the tube with the zero reference point at the initiating electrode. The voltage was measured on the flat portion of the probe voltage signal. As the distance from the electrode was increased, the probe voltage climbed sharply to a peak at 7.5 cm and then dropped off sharply until a constant value was reached at about 40 cm. The peaking of the voltage was caused by the O-ring coupling joint used to fasten the electrode assembly to the Pyrex tube. The nylon clamping material assumed the potential of the Pyrex tube and effectively increased its radius at that point. From the breakdown tube voltage profile curve, the axial position for the electrostatic probe was chosen to be 50 cm from the electrode. The voltage profile curves of Figure 15 were made on the mock-up apparatus with an applied voltage of +6 KV and the zero reference point located at the flat face of the cylindrical conductor. Two cylindrical conductors were used with outer diameters of 2.858 cm and 4.920 cm. The profiles have an inflection point occurring at the face of the conductors with the voltage decreasing to the left and increasing to the right with the maximum voltage at +5 cm for the 2.858 cm conductor and at +15 cm for the 4.920 cm conductor. The distance between the 10% and 90% points for the 4.920 cm conductor is approximately 28 cm which results in a 28 nanosecond rise time for a wave traveling at a velocity of

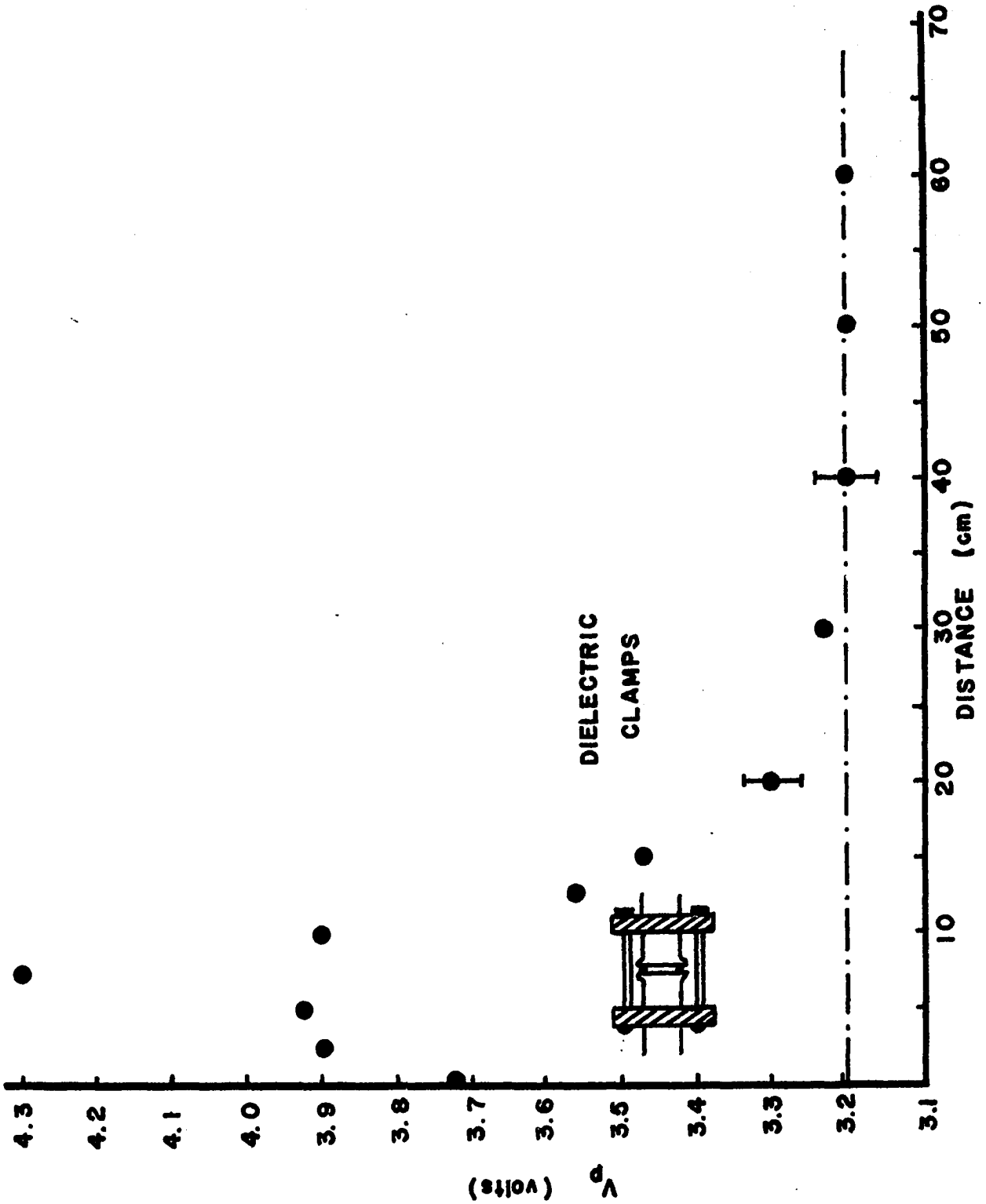

FIGURE 14. PROBE VOLTAGE PROFILE CURVE FOR THE BREAKDOWN TUBE.

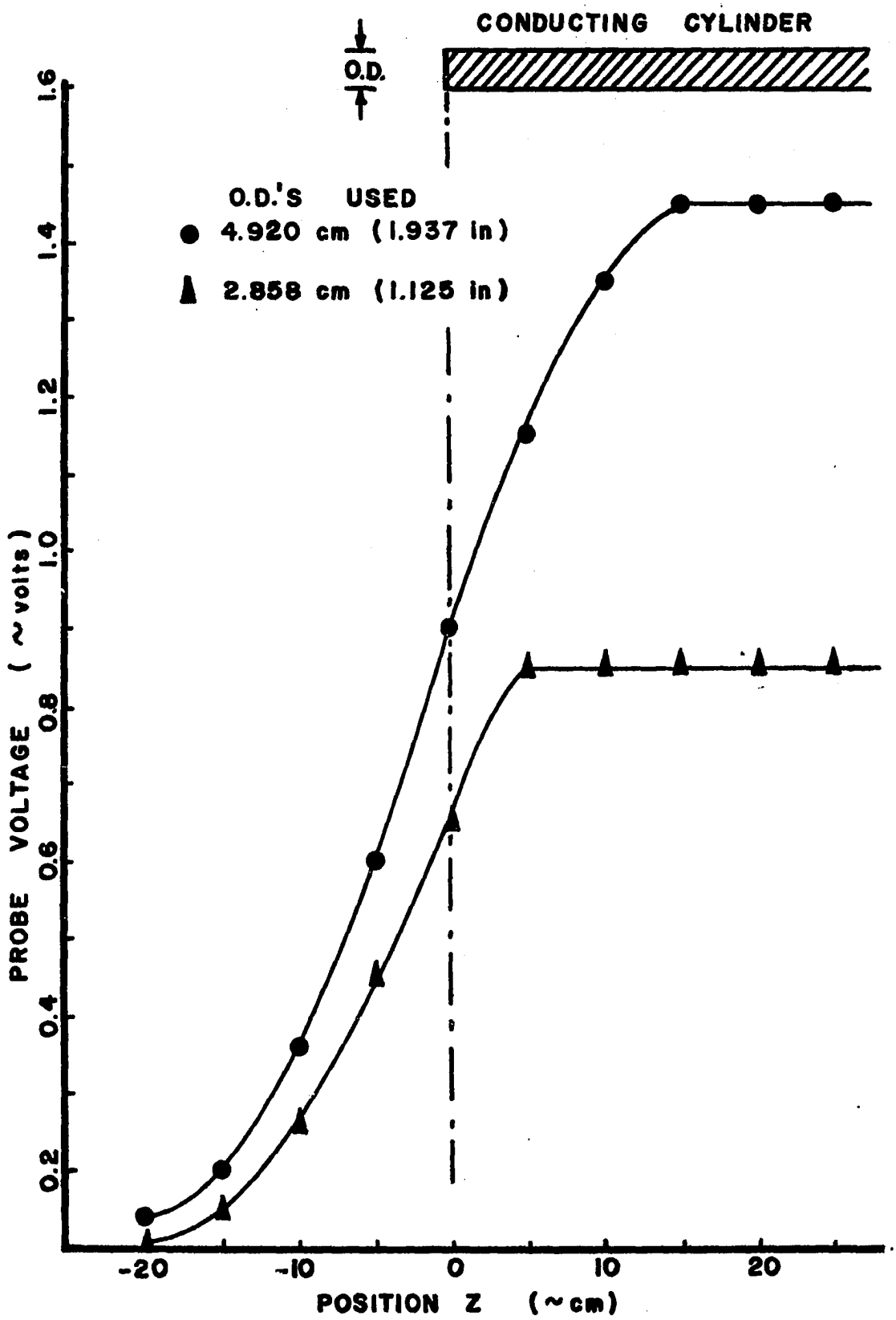

FIGURE 15. PROBE VOLTAGE PROFILE CURVES FOR THE MOCK-UP APPARATUS.

10^9 cm/sec. The axial position for the electrostatic probe was chosen to be +25 cm on the mock-up apparatus.

The second step in the calibration procedure was to find the relationship between the probe voltage and the applied voltage on the breakdown tube, and compare this to equivalent relationships on the mock-up apparatus for the 2.858 cm and 4.920 cm conductors. The data for the breakdown tube was taken prior to each data run on both nitrogen and argon gas and is illustrated in Figures 16 and 17. The procedure was to record the applied voltage and probe voltage for each data run at all gas pressures and then average the probe voltages taken at the same applied voltage separately for nitrogen and argon. The data for the antiforce wave (or positive applied voltages) presented in Figure 16 represents a linear relationship with a slope of 7.86×10^{-5} volts/volt. The proforce wave (or negative applied voltages) presented in Figure 17 was linear up to an applied voltage of about 40 KV where it began to curve off slightly. The nonlinearity above 40 KV was caused by the poor large signal response of the 2N2862 output transistor. The linear portion of the curve also had a slope of 7.86×10^{-5} and the approximate slope of the nonlinear portion was 6.43×10^{-5} volt/volt. Equivalent data was taken on the mock-up apparatus for the 2.858 cm and 4.920 cm O.D. conductors at applied voltages of ±6 KV, ±9 KV and ±12 KV and plotted on the curves of Figures 16 and 17. The data for the 4.920 cm O.D. conductor gives an exact fit with the data taken on the breakdown tube and is, therefore, the closest approximation to the plasma column.

The third and final step of the calibration procedure was to

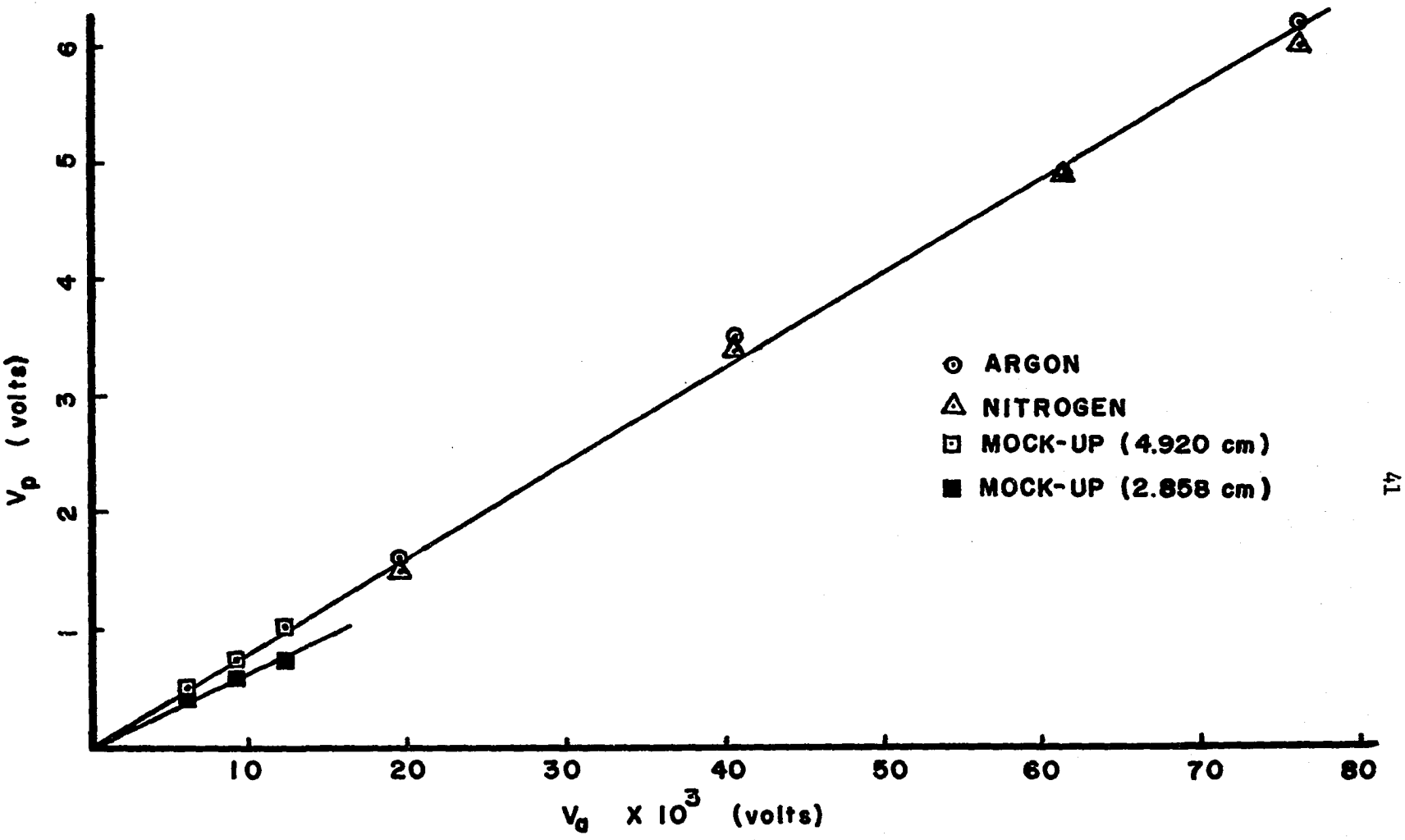

FIGURE 16. PROBE VOLTAGE VERSUS APPLIED VOLTAGE FOR NITROGEN AND ARGON ANTIFORCE WAVES.

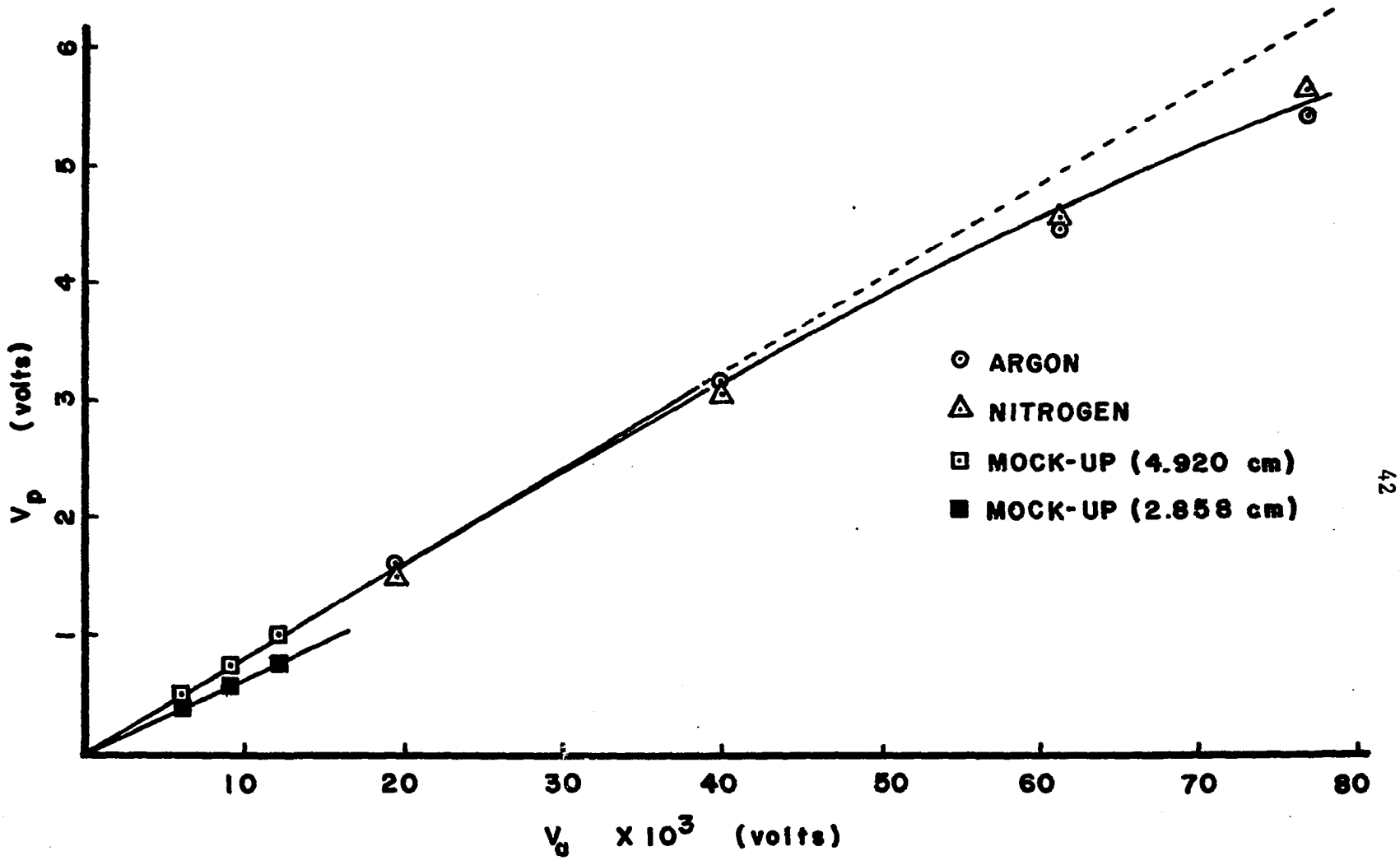

FIGURE 17. PROBE VOLTAGE VERSUS APPLIED VOLTAGE FOR NITROGEN AND ARGON PROFORCE WAVES.

relate the electric field (along the axis of the tube) to the potential at the wave's front. This was accomplished with a 75 cm long electrostatic probe inserted into the end of the mock-up apparatus opposite the conducting cylinder. The probe was fabricated from a piece of 50 ohm RG-58/U coax which was inserted into a section of glass tubing for rigidity. It was then aligned with the axis of the Pyrex tube as illustrated in Figure 13 by means of a styrofoam support. The distance from the face of the cylindrical conductor was measured from a centimeter scale attached to the electrostatic probe and a pointer located at the far end of the Pyrex tube. The probe was coupled to the oscilloscope by an additional 15 meters of RG-58/U coaxial cable without any impedance matching circuitry. For this reason, the signal was connected directly to the 1Meg input impedance of the scope, instead of the 50 ohm termination used with the probe coupling circuit. The reflections introduced at the leading edge of the probe signal due to the impedance mismatch were avoided by measuring the voltage at a point 2 μs later in time but still on the flat portion of the voltage signal. Based on the results of the previous steps only the 4.920 cm O.D. conductor was used in the final step of the calibration procedure. The selection of a flat faced geometry for the conductor resulted from the assumption that the wave front was a sharp discontinuity. The voltage profile curves of Figure 18 were taken with applied voltages of +6 KV, +9 KV and +12 KV along the center line of the Pyrex tube. The proportionality constant relating the electric field (E_z) at the face of the conductor to the applied voltage on the conductor was obtained from the curves in the following manner. The data points were fit by a French curve

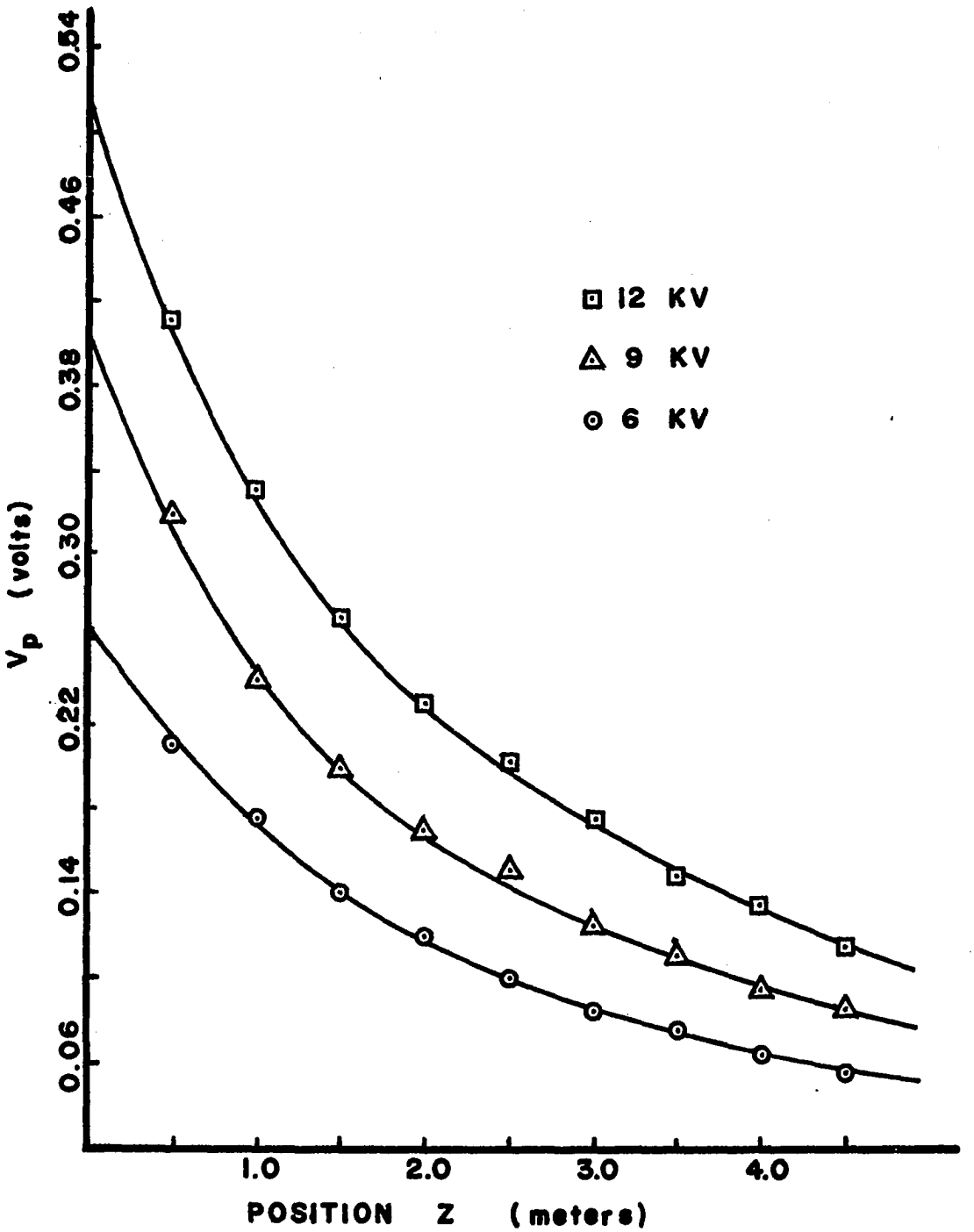

FIGURE 18. VOLTAGE PROFILE CURVES RELATING THE ELECTRIC FIELD TO THE APPLIED VOLTAGE.

with the condition that the point of intersection on the voltage axis be an inflection point on the French curve and the ratios of the voltages at the point of intersection be the same as the ratios of the corresponding applied voltages. The constant of proportionality was then calculated from the relationship

$$A_z = \frac{1}{v_0} \frac{\Delta v}{\Delta z} \tag{1}$$

where

v_0 = the voltage at the point of intersection

$\frac{\Delta v}{\Delta z}$ = the slope of the curve at the point of intersection.

The average value of the proportionality constant calculated for the three curves was found to be 0.454 cm^{-1} which is 2.24 times larger than the theoretical value calculated by Babb. The difference is due to the influence of the dielectric constant introduced by the Pyrex tube which was not inlcuded in the calculation of Babb. The electric field at the front of the wave can now be calculated from the expression

$$E_z = \left(\frac{A_z}{A_r}\right) v_p \tag{2}$$

where A_r was the proportionality constant relating the probe voltage to the wave voltage and v_p was the probe voltage measured at the point of maximum slope change on the leading edge of the detected signal as illustrated in the sketch below. The voltage droop at the leading edge of the probe signal was caused by collisional damping of the current

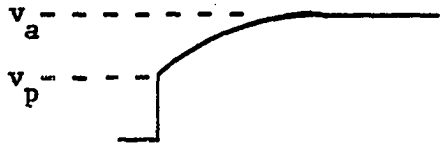

feeding the electric field at the front and was the source of the wave speed decrement β. It should be mentioned at this point that all the data used in the graphical analysis of the electrostatic probe is presented in tabular form in Appendix A.

C. Experimental Results

Applying the techniques described in the previous sections to raw data of argon and nitrogen for both proforce and antiforce waves gives the results illustrated in Figures 19 through 22. The instantaneous velocities calculated by the computer program of Appendix C are plotted against the reduced electric field E/p, where E was calculated using equation 2 of section B. The raw data used in these calculations is given in tabular form in Appendix B.

Three features previously reported by Blais are observed in the present experiment. First, the pressure dependence of the wave speeds is analogous to the Paschen curve, which does not however imply that the two phenomenon are related, but only that for a given field strength there is a pressure at which maximum speed occurs. The peak pressure for both argon and nitrogen was around 1.0 torr, in contrast to a pressure of 3.0 torr for helium as reported by Blais. Second, at very low pressures in the antiforce case the wave speed approaches a constant value independent of the electric field. Finally, a stepped-leader phenomenon was observed in the time of flight measurements which resulted in some uncertainty of the wave speeds. This phenomenon was most pronounced at pressures below a few torr. It was not specifically investigated.

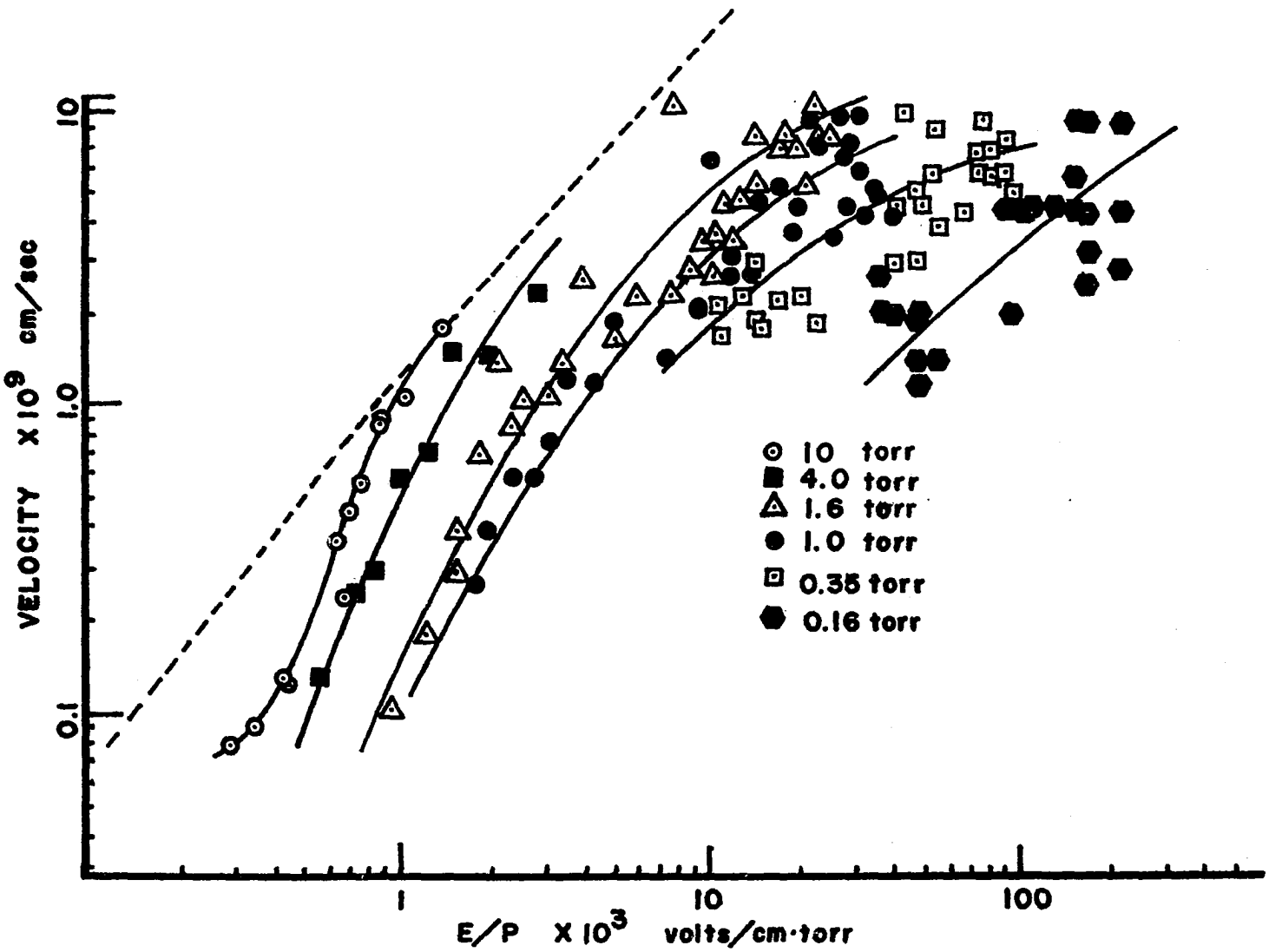

FIGURE 19. PROFORCE CURVES FOR NITROGEN GAS.

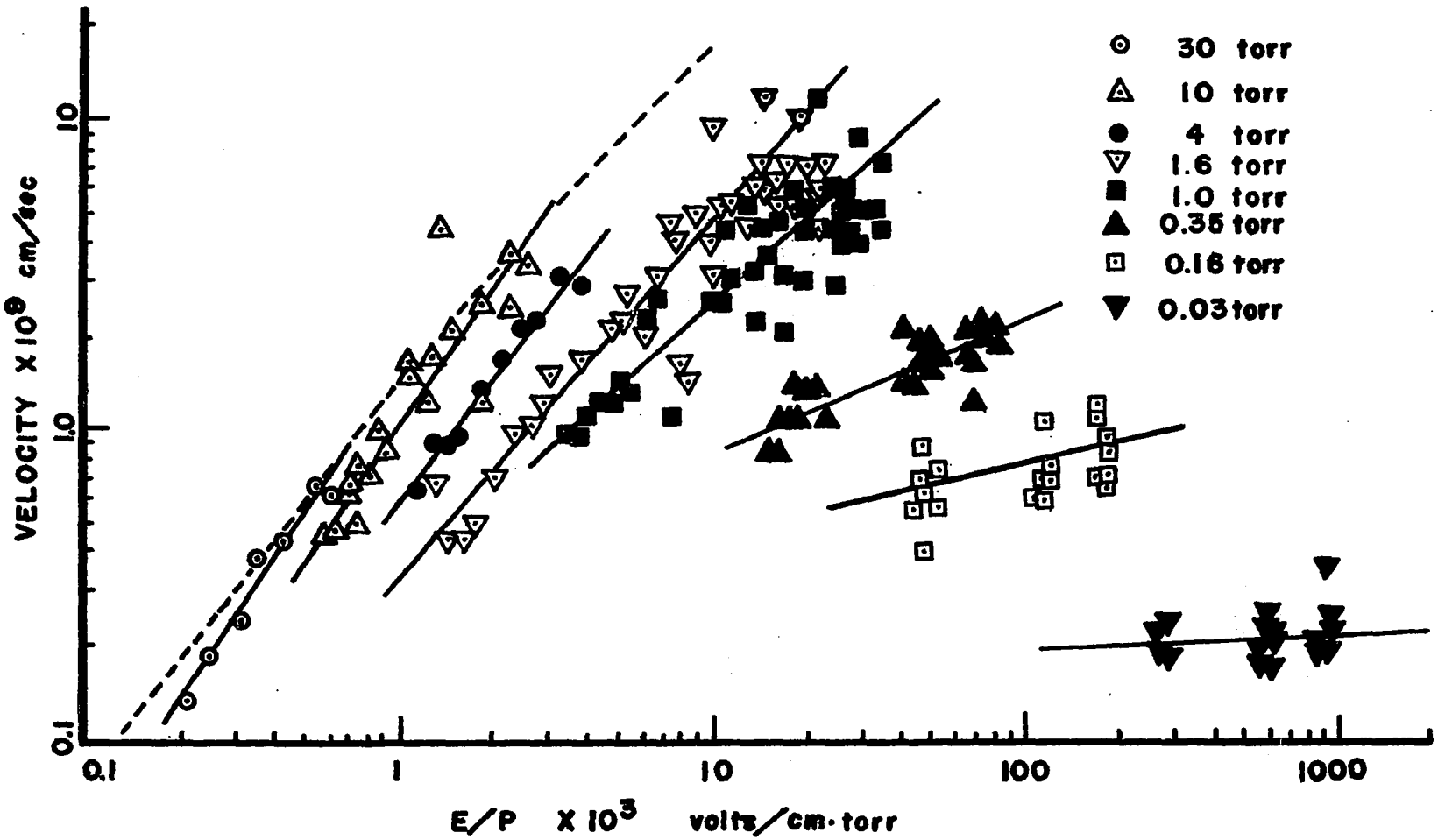

FIGURE 20. ANTIFORCE CURVES FOR NITROGEN GAS.

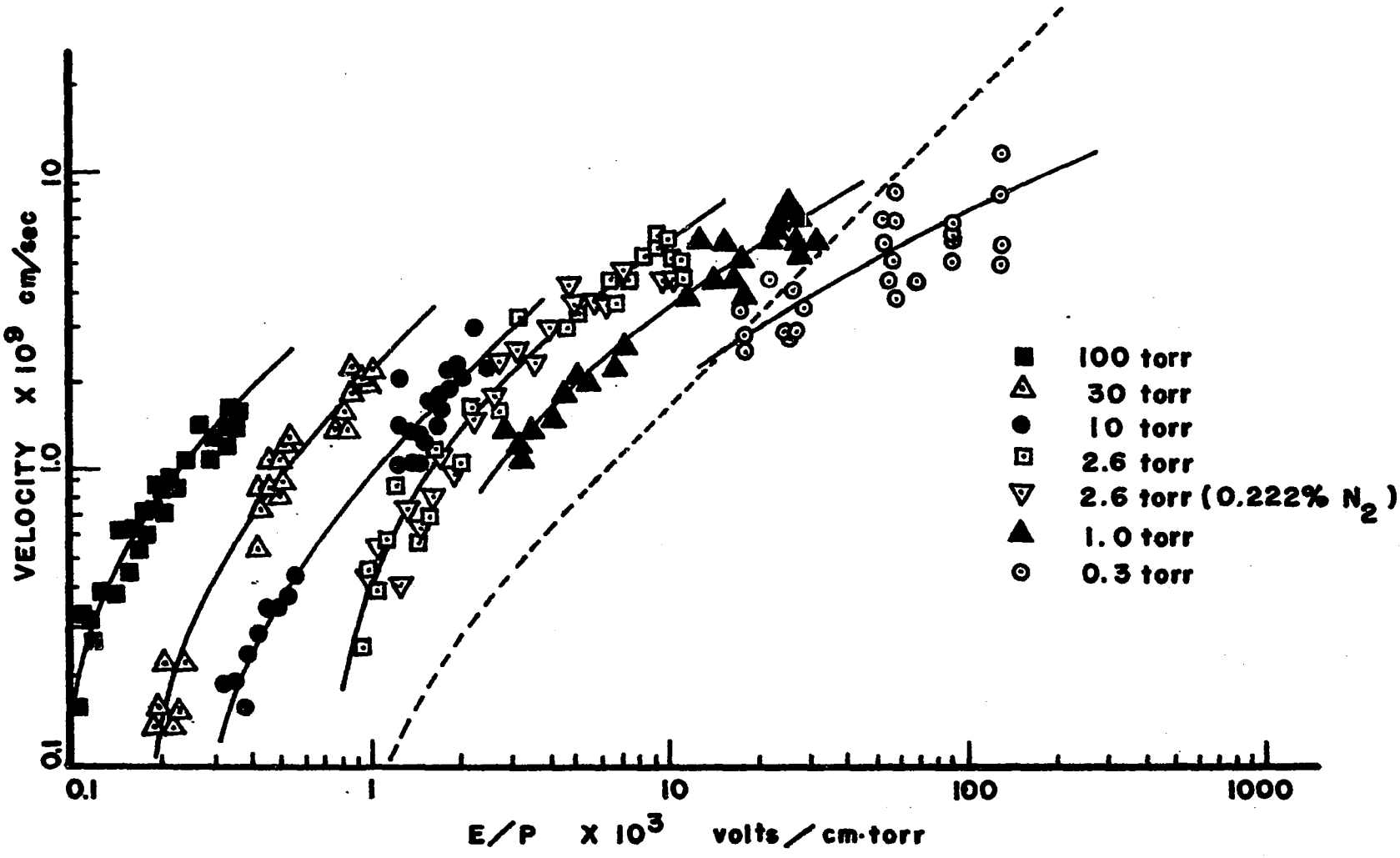

FIGURE 21. PROFORCE CURVES FOR ARGON GAS.

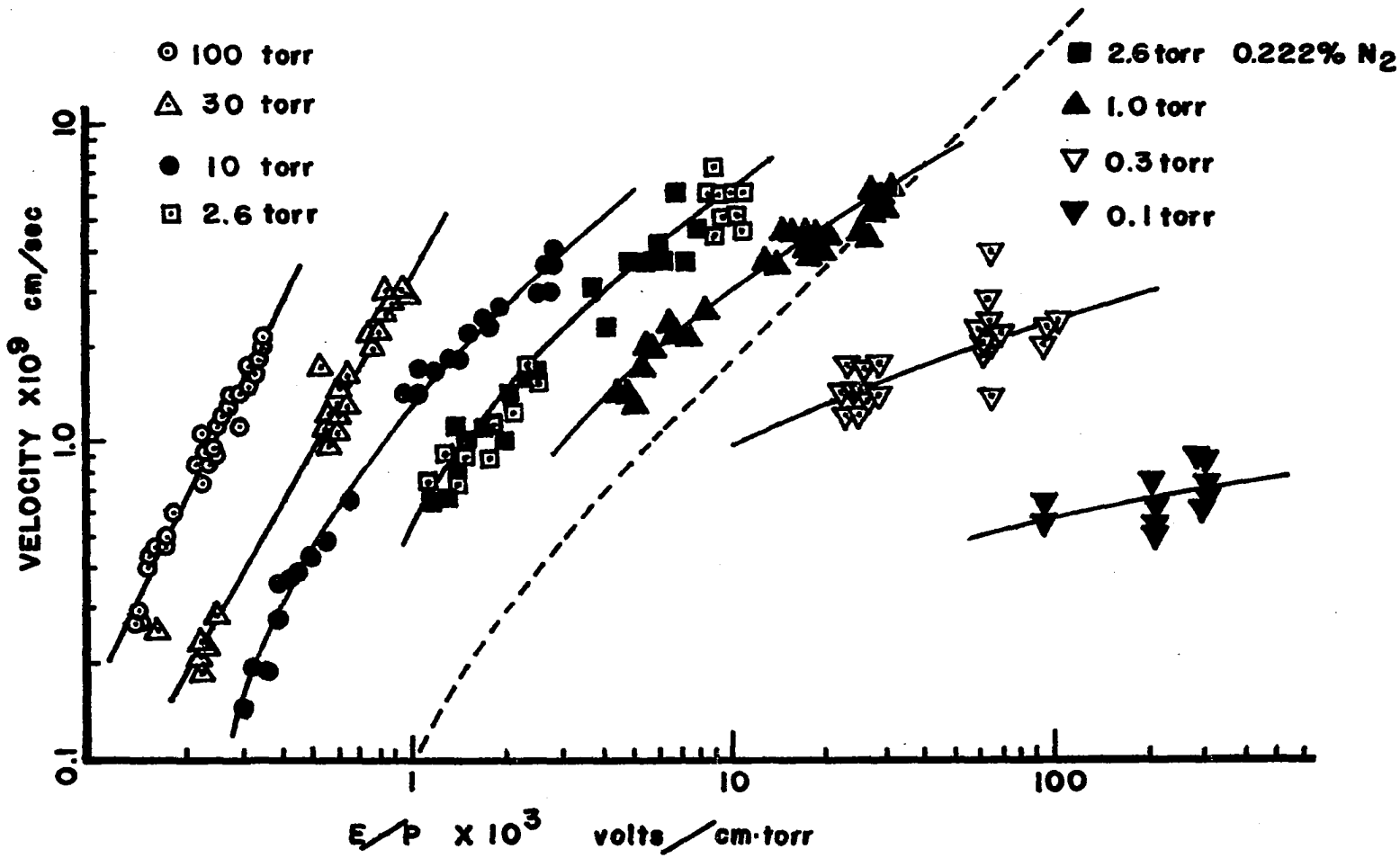

FIGURE 22. ANTIFORCE CURVES FOR ARGON GAS.

There were three additional effects observed in these experiments. First, there is an upper limit for the wave speed on the order of 10^{10} cm/sec. The exact value was not ascertained because of the statistical scatter of the data. Second, at low pressures for negative applied voltages two progressive phenomena were clearly distinguished by the electrostatic probe and the photomultipliers. The second phenomenon was easily identified by its sharp front as the strong proforce wave described by Shelton. This was preceded by a phenomenon characterized by a gradual buildup in potential and light intensity. This may be the weak proforce wave postulated by Fowler[10] (based on a previous observation by this author) or a Townsend avalanche of electrons. It is quite possible that above the Shelton initial velocity this phenomenon always undergoes transition to the strong proforce wave at some point in time which may occur too early at higher pressures to be observed. For positive applied voltages only one phenomenon was observed which is consistent with the Sanmann theory that denies the existence of strong antiforce waves. Finally, there was a distinct difference in the range of pressures for which wave initiation occurred in argon and in nitrogen. The pressure range for argon was from 0.1 torr to 100.0 torr in the antiforce case and from 0.3 torr to 100.0 torr in the proforce case. The range for nitrogen was from 0.03 torr to 30.0 torr in the antiforce case and 0.16 torr to 10.0 torr in the proforce case. In the proforce case, the minimum pressure was the lowest pressure at which strong waves could be recognized in this apparatus.

D. Comparison to Theory

A relationship between the velocity and the reduced electric field can be found in the Shelton and Sanmann theories and compared to the experimental results obtained for argon and nitrogen. The expression from both theories is

$$\frac{E_0}{p} = \frac{m}{e\kappa}\left(\frac{K_1}{p}\right)V_0 \qquad (1)$$

where κ is a dimensionless parameter and K_1 is the electron collision frequency of the gas. The term (K_1/p) is independent of pressure for the range of velocities under consideration, and is found from tables by Jayroe[11] to be a constant value of 8.28×10^9 $sec^{-1}torr^{-1}$ for argon and 8.94×10^8 $sec^{-1}torr^{-1}$ for nitrogen. Plots of Eq. 1 are illustrated on the experimental curves by the dashed line.

Since Eq. 1 is independent of pressure the best fit with the experimental data should occur around 1.0 torr. The large disagreement in nitrogen is because the theories do not account for energy loss in the rotational vibration modes of molecules. Reasonable agreement is achieved with argon which is off by only a factor of two, which can easily be accounted for by the uncertainty in the location of the wave front on the rise time of the probe signal as illustrated in Figure 15. The point of maximum slope change on the leading edge of the probe signal was arbitrarily chosen for ease of measurement. Therefore, the factor of two agreement is quite good.

The remaining pressure dependence of the experimental curves must be explained by analysis of the theory and experiment together. First, the presence of the Pyrex tube wall requires that the collision

frequency of the gas (K_1) be replaced by an effective collision frequency of the gas and wall. From Shelton's theory we have

$$K_1\lambda = \bar{v} \tag{2}$$

where λ is the mean free path of the gas and $\bar{v}$ is the electron drift velocity in the wave front. Since the electron drift velocity will remain unchanged with the introduction of the tube wall, Eq. 2 can be rewritten as

$$K_1'\lambda' = \bar{v} \tag{3}$$

where λ' is the effective mean free path of the gas and wall combination and can be approximated as

$$\frac{1}{\lambda'} = \frac{K_1}{\bar{v}} + \frac{2.4}{a} . \tag{4}$$

Substituting Eq. 4 into Eq. 3 and rearranging gives

$$K_1' = K_1 + 2.4\,\frac{\bar{v}}{a} . \tag{5}$$

Now, replacing K_1 by K_1' in Eq. 1 and solving for E_0 yields

$$\frac{E_0}{p} = \frac{m}{e\kappa}\left(\frac{K_1}{p} + 2.4\,\frac{\bar{v}}{ap}\right) . \tag{6}$$

The drift velocity is expressed in terms of the electron temperature as

$$\bar{v} = \left(\frac{3kT_e}{m}\right)^{\frac{1}{2}} \tag{7}$$

and the electron temperature is related to the wave velocity by

$$T_e = \frac{mb}{k}\,V_0^2 . \tag{8}$$

Combining Eqs. 7 and 8 yields

$$\bar{v} = \sqrt{3b}\;\; V_0 \tag{9}$$

where $b = 0.2$ for proforce waves;

$b = 0.6$ for antiforce waves.

Finally, inserting Eq. 9 into Eq. 6 gives

$$\frac{E_0}{p} = A\, V_0 + \left(\frac{B}{p}\right) V_0^2 \qquad (10)$$

where

$$A = \frac{m}{e\kappa}\left(\frac{K_1}{p}\right)$$

$$B = \frac{2.4m\sqrt{3b}}{ea\kappa}$$

The second term of Eq. 10 introduces a pressure dependence below 1.0 torr where the mean free path of the gas becomes comparable with the dimensions of the tube, but does not account for the high pressure region. There is no modification to the theory that can be made to account for the high pressure dependence, therefore, it must be assumed that the error is not in the theory but lies in the experiment itself.

It is a well known fact that a plasma column constricts with increasing pressure but none was noted during the probe calibration procedure. The plasma column appeared to fill the tube at all pressures which is inconsistent with the known facts. In the calibration procedure the droop in the probe signal at high pressures was initially assumed to be a result of increased plasma resistance. The flat region of the signal was thought to be when the quasineutral region behind the front had attained the potential of the electrode. In retrospect, it was probably a result of electron diffusion capacitively charging the glass wall to the potential of the constricted plasma. The charged tube then shielded the plasma potential from the probe and produced a higher probe voltage by effectively increasing the radius of the inner conductor. This explains why the 4.920 cm O.D. conductor on

the mock-up fit perfectly with the breakdown tube data for all pressures. Based on this analysis, a technique was sought to recover the pressure dependence of the electric field from the experimental data. This was accomplished by drawing a line through the experimental data at a constant velocity of 10^9 cm/sec and plotting the value of E/p obtained from each curve as a function of pressure. For argon this resulted in a pressure dependence for E/p of $p^{-\frac{1}{2}}$ instead of p^{-1} which would have been the case if E were independent of pressure. Using this method, the pressure dependence of the electric field due to plasma constriction was found to be

$$E = E_{ob}\left[1 + \left(\frac{p}{p_c}\right)^{\frac{1}{2}}\right] \tag{11}$$

At this point it is simpler to incorporate Eq. 11 into the theoretical expression of Eq. 10 than it is to recalculate the electric fields of the experiment. The final expression then becomes

$$\frac{E_{ob}}{p} = \frac{A\,V_0 + B\left(\frac{V_0^2}{p}\right)}{1 + \left(\frac{p}{p_c}\right)^{\frac{1}{2}}} \tag{12}$$

The expression gives good agreement for the proforce case of argon at all pressures for $A = 2.53 \times 10^{-6}\ \frac{\text{volt}\cdot\text{sec}}{\text{cm}^2\cdot\text{torr}}$, $B = 7.76 \times 10^{-16}\ \frac{\text{volts}\cdot\text{sec}^2}{\text{cm}^3}$ and $p_c = 1.0$ torr. In the antiforce case there is good agreement at high pressures but still not for pressures below 1.0 torr. This strong pressure dependence below 1.0 torr was also observed (but not measured) for the weak proforce wave. The pressure dependence in this region is apparently more complicated than this simple correction term predicts. Also, the theoretical expression does not predict the curvature or maximum velocity of the experimental results.

CHAPTER IV

CONCLUSIONS AND SPECULATIONS

This experiment has been successful in resolving the major discrepancies between experiment and theory for the propagation of breakdown waves in atomic gases. The high pressure dependence of the experimental results was found to be caused by constriction of the plasma column. The constriction introduced a pressure dependence into the observations which was previously overlooked by Blais and Haberstich. Agreement in the unconstricted low pressure region was improved by incorporating an additional term in the theory to allow for the influence of the confining tube. The energy of the electrons in the wave is decreased as a result of electron collisions with the tube wall. The additional term in the theory was derived by assuming a collision frequency for the electrons with the tube wall in order to account for the energy lost in this process.

The experiment also revealed an upper limit in the wave speed of approximately one-third the speed of light. The theories do not predict this upper limit in the speed which is perhaps a relativistic effect not included in the simplified theories. Also the curvature of the wave speed data at low velocities is not predicted by the current theories, probably because they use thermal production of ionization only.

The scatter in the wave speed data at low pressures was a result of the wave appearing to speed up and then slow down between successive distance intervals during a data run. A possible explanation for this phenomenon is the leader effect which was proposed by Blais. This fluctuation might be reduced by increasing the distance interval used in the wave speed measurements. An alternate method would be to reduce the size of the glass tube by a factor of two which would have the effect of doubling the length of the entire apparatus. Better still might be the use of image converter studies of the wave speed.

In conclusion, it can be stated that the one dimensional theories of Shelton and Sanmann are good central approximations of the breakdown process which give excellent agreement for atomic gases. Molecular gases will require a modification of the theory which allows for the energy lost to rotational vibration modes of the molecules. In addition, it is concluded that contamination levels of a few tenths of a percent have no effect on the propagation of the breakdown wave.

BIBLIOGRAPHY

1. F. Hauksbee, Philosophical Transactions of the Royal Society XXV (Issue 307), 2277-2282 (1706).
2. G. W. Paxton and R. G. Fowler, Phys. Rev. 128:993 (1962).
3. A. Haberstich, "Experimental and Theoretical Study of An Ionizing Potential Wave in a Discharge Tube", Ph.D. Dissertation, University of Maryland (1964).
4. G. A. Shelton, "An Investigation into the Structure of Electron Fluid-Dynamical Waves", Ph.D. Dissertation, University of Oklahoma (1967).
5. E. Sanmann, "Antiforce Electron Dynamical Waves", Ph.D. Dissertation, University of Oklahoma (1974).
6. R. Blais, "The Electrical Breakdown of Helium", Ph.D. Dissertation, University of Oklahoma (1971).
7. I. D. Latimer, J. I. Mills and R. A. Day, J. Quant. Spectrosc. Radiat. Transfer 10:629 (1970).
8. G. E. Copeland, "Lifetimes of Excited Electronic States of Chemically Active Gases", Ph.D. Dissertation, University of Oklahoma (1970).
9. S. E. Babb, Jr., private communication.
10. R. G. Fowler, Adv. in Electronics and Electron Phys. 35:53 (1974).
11. R. Jayroe, Adv. in Electronics and Electron Phys. 35:64 (1974).

APPENDIX A

This appendix presents in tabular form the raw data used in the calibration of the electrostatic probe. The data is illustrated in graphical form in Figures 14 to 18 of Chapter III. The tabulated form of the data is included in the dissertation to aid in any future analysis of the experimental results.

Distance from electrode (cm)	0	5	7.5	10	12.5	15	20	30	40	50	60
Probe voltage (volts)	3.72	3.9	4.3	3.9	3.56	3.47	3.3	3.23	3.2	3.2	3.2

TABLE 1. PROBE VOLTAGE VERSUS POSITION ON THE SIDE OF THE BREAKDOWN TUBE.

	Applied voltage (volts)	Probe voltage for nitrogen (volts)	Probe voltage for argon (volts)
Antiforce	19.72	1.55	1.60
	40.60	3.35	3.40
	61.48	4.92	4.93
	76.56	6.00	6.20
Proforce	19.72	1.55	1.60
	40.14	3.04	3.15
	61.25	4.55	4.47
	77.14	5.65	5.40

TABLE 2. BREAKDOWN TUBE APPLIED VOLTAGE VERSUS PROBE VOLTAGE AT z=50 cm.

Position on side of tube (cm)	-20	-15	-10	-5	0	+5	+10	+15	+20	+25
Probe voltage (volts)	0.14	0.20	0.36	0.60	0.90	1.15	1.35	1.45	1.45	1.45

TABLE 3. PROBE VOLTAGE VERSUS POSITION ON SIDE OF MOCK-UP RELATIVE TO THE FLAT FACE OF THE CONDUCTOR.

Applied Voltage (KV)	Probe voltage for 1.125" conductor (volts)	Probe voltage for 1.937" conductor (volts)
±6	0.40	0.56
±9	0.60	0.75
±12	0.75	1.03

TABLE 4. APPLIED VOLTAGE VERSUS PROBE VOLTAGE ON THE MOCK-UP AT z=25 cm.

Distance from conductor (cm)	Probe voltage in volts for applied voltages of		
	6 KV	9 KV	12 KV
0.5	0.210	0.320	0.410
1.0	0.175	0.242	0.330
1.5	0.140	0.200	0.270
2.0	0.120	0.170	0.230
2.5	0.100	0.150	0.203
3.0	0.085	0.125	0.175
3.5	0.074	0.110	0.150
4.0	0.063	0.095	0.135
4.5	0.056	0.086	0.116

TABLE 5. ELECTRIC FIELD PROPORTIONALITY CONSTANT DATA FOR 1.937" O.D. CYLINDRICAL CONDUCTOR.

APPENDIX B

ELECTRIC FIELD AND WAVE SPEED RAW DATA FOR NITROGEN AND ARGON

The table below presents the raw data for the electric field and wave speed measurements in the form of probe voltage (in volts) and normalized elapsed time (in nanoseconds) as a function of the position z along the tube. The normalized time intervals were calculated in the computer program by subtracting the first time interval from all successive intervals. The probe voltages were recorded directly from a Tektronix dual beam oscilloscope. Unless otherwise indicated, the start trigger for the wave speed measurements was located at the 1.0 meter viewport. The probe voltages of ±20 KV, ±40 KV and ±60 KV for the 1.6 torr pressure and of ±20 KV and ±40 KV for the 1.0 torr pressure of nitrogen were measured with the unattenuated mode of the E.S. probe and have a different value for A_r at 1.17×10^{-4} volts/volt. All other probe measurements were taken on the 2 to 1 attenuation mode at the E.S. probe and use the A_r constant stated in the text.

Nitrogen - Proforce

Press (torr)	Volt (KV)	Item	z (meters) → 1.5	2.0	2.5	3.0	3.5	4.0	4.5	5.0	5.5	6.0	6.5
10	-60	PROBE	-	-	1.5	1.3	1.1	0.7	0.5	0.5			
		TIME	-	-	0	69.1	178.6	347.0	820.5	1601.0			
	-80	PROBE	-	2.4	1.8	1.5	1.2	1.0	0.7	0.6	0.6		
		TIME	-	0	33.2	90.6	159.3	292.0	542.7	1013.0	1654.0		
4	-40	PROBE	2.0	1.5	1.1	0.9	0.7	0.6	0.5	0.4	0.3		
		TIME	0	24.5	64.7	105.0	188.7	285.2	488.7	726.3	1169.6		
1.6	-20	PROBE	1.48	1.06	0.97	0.81	0.81	0.63	0.49	0.45	0.4		
		TIME	0	54.7	96.7	183.9	334.8	536.8	853.1	1434.0	-		
	-40	PROBE	5.17	4.63	3.83	3.11	2.58	2.0	1.7	1.5	1.3	1.2	1.1
		TIME	0	20.9	40.4	64.1	87.4	121.1	142.5	185.9	237.2	290.2	354.2
	-60	PROBE	8.0	7.5	7.0	6.5	6.0	5.5	5.0	4.0	3.6	3.2	2.8
		TIME	0	10.1	18.5	29.4	41.5	53.2	68.2	83.7	89.5	126.3	143.6
	-80	PROBE	5.6	5.2	5.0	4.8	4.4	4.0	3.6	3.2	2.8	2.6	2.4
		TIME	0	7.2	14.4	20.2	30.3	37.5	44.7	53.4	60.6	76.4	-
1.0	-20	PROBE	1.9	1.5	1.3	1.1	0.9	0.8	0.7	0.6	0.5	0.46	0.4
		TIME	0	40.7	65.3	95.2	142.4	188.6	263.4	359.9	455.6	598.2	812.1
	-40	PROBE	4.8	4.6	4.2	3.8	3.5	3.2	3.0	2.6	2.4	2.0	2.0
		TIME	0	14.9	22.8	32.9	44.4	64.6	68.7	86.0	94.6	120.5	143.6

Nitrogen - Proforce

Press (torr)	Volt (KV)	Item	z (meters) → 1.5	2.0	2.5	3.0	3.5	4.0	4.5	5.0	5.5	6.0	6.5
1.0	-60	PROBE	4.6	4.4	4.2	4.0	3.6	3.4	3.2	3.0	2.8	2.4	2.2
		TIME	0	12.2	17.6	24.3	32.5	46.9	51.2	58.4	64.2	75.8	85.6
	-80	PROBE	5.6	5.4	5.2	5.0	4.8	4.6	4.4	4.2	4.0	3.8	3.6
		TIME	0	12.2	14.2	18.9	29.5	39.6	42.5	51.1	54.0	65.6	71.3
0.35	-20	PROBE	1.35	1.2	1.0	0.9	0.9	0.85	0.75	0.65	0.65	0.65	0.6
		TIME	0	27.4	50.3	73.3	102.1	128.0	145.3	168.0	192.1	222.2	252.4
	-40	PROBE	3.3	3.2	3.1	3.0	2.9	2.8	2.6	2.4	2.3	2.2	2.0
		TIME	0	13.5	20.1	28.8	40.3	57.6	67.7	73.3	90.6	102.1	-
	-60	PROBE	4.8	4.6	4.4	4.2	4.0	3.8	4.0	3.8	3.4	4.0	3.8
		TIME	0	10.1	16.9	25.7	34.4	43.0	50.2	57.5	63.2	74.8	78.9
0.16	-20	PROBE	1.5	1.3	1.3	1.2	1.2	1.2	1.1	1.0	1.0	1.0	1.0
		TIME	0	34.6	69.1	103.6	129.0	171.2	195.3	219.4	237.5	261.6	-
	-40	PROBE	3.2	3.2	3.2	3.2	3.1	3.0	3.0	2.8	2.6	2.5	2.8
		TIME	0	20.2	31.7	43.2	54.7	66.2	77.7	89.3	100.8	126.3	138.4
	-60	PROBE	4.8	4.8	4.8	4.7	4.7	4.6	4.2	4.2	4.2	4.0	4.2
		TIME	0	17.3	23.0	34.6	48.9	60.5	66.2	74.9	80.6	92.1	-

Nitrogen - Antiforce

Press (torr)	Volt (KV)	Item	z (meters) → 1.5	2.0	2.5	3.0	3.5	4.0	4.5	5.0	5.5	6.0	6.5
30	+80	PROBE	3.2	2.8	2.2	1.8	1.6	1.3	1.1	0.9	-	-	-
		TIME	0	93.5	181.6	314.2	464.2	701.8	1025.5	1471.4	-	-	-
10	+60	PROBE	3.9	3.2	2.6	2.2	1.9	1.6	1.4	1.2	1.1	1.0	0.9
		TIME	0	21.6	43.3	69.2	102.1	139.6	206.0	284.4	374.9	482.2	601.1
	+80	PROBE	4.6	4.0	3.2	2.4	2.2	1.9	1.5	1.3	1.2	1.1	1.0
		TIME	0	16.9	31.5	77.6	90.4	136.4	171.0	225.9	298.3	382.7	502.2
4.0	+40	PROBE	2.7	2.3	1.9	1.7	1.5	1.3	1.1	1.0	0.9	0.8	0.7
		TIME	0	18.8	36.1	60.4	86.3	117.9	161.1	217.1	277.4	337.8	421.7
1.6	+20	PROBE	2.3	1.8	1.7	1.6	1.4	1.2	1.1	1.0	0.9	0.8	0.7
		TIME	0	31.7	67.4	111.1	163.3	224.8	300.8	406.2	526.2	646.2	724.7
	+40	PROBE	6.6	6.0	5.2	4.8	4.3	4.0	3.6	3.2	3.1	2.9	2.6
		TIME	0	17.3	33.7	44.3	77.1	88.6	105.9	131.8	150.8	174.4	199.7
	+60	PROBE	9.5	8.8	8.2	7.5	7.0	6.5	6.0	5.5	5.0	4.5	4.0
		TIME	0	8.7	13.3	22.2	32.3	42.7	53.2	66.4	72.2	110.8	124.0
	+80	PROBE	6.0	5.8	5.4	5.2	5.0	4.7	4.4	4.0	3.6	3.2	-
		TIME	0	7.2	16.6	23.8	28.8	38.9	46.1	56.2	63.4	75.0	-
1.0	+20	PROBE	2.2	2.0	1.8	1.6	1.5	1.4	1.3	1.2	1.1	1.0	0.9
		TIME	0	47.6	67.6	90.6	130.9	166.9	209.1	251.4	299.6	353.9	408.2

Nitrogen - Antiforce

Press (torr)	Volt (KV)	Item	z (meters) → 1.5	2.0	2.5	3.0	3.5	4.0	4.5	5.0	5.5	6.0	6.5
1.0	+40	PROBE	5.3	5.1	4.9	4.6	4.3	4.0	3.6	3.5	3.5	3.2	3.0
		TIME	0	16.2	27.1	41.5	53.0	76.1	86.0	103.3	103.3	134.9	155.1
	+60	PROBE	4.8	4.6	4.4	4.2	4.1	3.8	3.6	3.5	3.5	3.2	3.0
		TIME	0	12.2	21.6	31.9	43.4	60.7	65.1	76.6	76.6	103.8	112.4
	+80	PROBE	6.0	6.0	5.7	5.2	5.1	5.2	4.8	4.6	4.6	4.2	3.6
		TIME	0	11.5	18.3	28.3	38.4	51.4	57.2	67.3	67.3	88.7	97.3
0.35	+20	PROBE	1.4	1.3	1.25	1.15	1.15	1.10	1.05	1.0	1.0	0.95	0.95
		TIME	0	48.9	86.4	123.8	160.9	209.1	257.4	305.6	305.6	389.8	449.2
	+40	PROBE	3.3	3.2	3.1	3.0	2.9	2.8	2.7	2.6	2.6	2.5	2.5
		TIME	0	30.3	59.1	92.0	118.0	143.9	174.7	210.8	235.0	271.2	307.3
	+60	PROBE	5.0	4.6	4.8	4.6	4.6	4.5	4.2	4.1	4.1	4.0	4.0
		TIME	0	27.4	53.4	77.7	103.6	129.5	152.5	183.6	207.7	237.8	280.1
0.16	+20	PROBE	1.45	1.4	1.4	1.3	1.3	1.3	1.3	1.3	1.25	1.3	1.25
		TIME	0	86.4	154.4	238.9	311.2	370.7	453.9	537.1	620.3	715.3	846.6
	+40	PROBE	3.4	3.4	3.3	3.3	3.3	3.3	3.2	3.1	3.1	3.1	3.1
		TIME	0	66.2	135.3	183.5	267.9	340.3	405.7	477.0	548.2	631.4	702.7
	+60	PROBE	5.0	5.1	5.0	4.9	5.0	5.0	4.8	4.8	4.8	4.8	4.8
		TIME	0	57.6	83.5	176.9	225.2	297.5	357.9	405.3	476.6	547.9	619.2

Nitrogen - Antiforce

Press (torr)	Volt KV)	Item	z (meters) →								
			1.5	2.0	2.5	3.0	3.5	4.0	4.5	5.0	5.5
0.3	+20	PROBE	1.5	1.5	1.4	1.4	1.4	1.4	1.4	1.4	
		TIME	0	273.3	475.3	739.5	962.4	1185.4	1408.4	1631.3	
	+40	PROBE	3.3	3.3	3.2	3.2	3.1	3.1	3.0	3.0	2.9
		TIME	0	225.8	463.4	677.3	978.0	1173.1	1396.0	1674.7	1925.5
	+60	PROBE	4.9	5.0	4.8	4.8	4.8	4.7	4.6	4.5	4.4
		TIME	0	235.2	438.2	640.2	916.3	1055.6	1306.5	1585.1	1836.0

Argon - Proforce

Press (torr)	Volt (KV)	Item	z (meters) → 1.5	2.0	2.5	3.0	3.5	4.0	4.5	5.0	5.5	6.0	6.5
100	-40	PROBE	2.8	2.6	2.5	2.4	2.3	2.2	2.0	1.9	1.8	1.7	1.6
		TIME	0	100.8	220.5	305.2	447.8	590.4	733.0	937.8	1105.0	1272.2	1606.6
	-60	PROBE	4.0	3.8	3.6	3.4	3.4	3.2	3.2	3.0	3.0	2.8	2.8
		TIME	0	48.9	106.5	161.4	221.7	294.1	354.4	425.8	509.0	580.3	663.5
	-80	PROBE	5.1	5.0	4.8	4.8	4.6	4.6	4.2	4.1	4.0	3.9	3.8
		TIME	0	33.2	70.4	107.9	139.5	182.9	225.1	267.4	315.6	363.8	399.8
30	-20	PROBE	1.2	1.15	1.1	1.05	1.0	0.95	0.9	-	-	-	-
		TIME	0	228.7	585.2	981.0	1204.0	1538.4	1928.5	-	-	-	-
	-40	PROBE	2.7	2.7	2.6	2.5	2.5	2.4	2.3	2.2	2.2	2.1	2.0
		TIME	0	40.3	83.5	141.1	203.4	251.6	311.9	360.3	431.6	491.0	586.0
	-60	PROBE	4.2	4.0	3.9	3.8	3.7	3.6	3.6	3.5	3.4	3.4	3.2
		TIME	0	23.1	49.0	76.2	105.0	133.8	156.8	188.7	224.9	261.1	297.2
10	-20	PROBE	1.0	0.9	0.8	0.75	0.7	0.65	0.65	0.6	0.55	0.5	-
		TIME	0	121.1	265.9	421.2	575.6	767.7	990.6	1325.1	1603.7	1882.4	-
	-40	PROBE	3.0	2.8	1.7	2.6	2.5	2.4	2.4	2.2	2.1	2.1	2.2
		TIME	0	28.8	58.9	102.1	139.5	188.7	224.9	273.1	309.3	357.6	381.8
	-60	PROBE	4.3	3.8	3.5	3.4	3.2	3.1	3.1	3.0	2.9	2.8	2.7
		TIME	0	23.1	40.4	64.7	87.7	110.8	133.8	162.6	194.5	230.6	260.8

Argon - Proforce

Press (torr)	Volt (KV)	Item	z (meters) → 1.5	2.0	2.5	3.0	3.5	4.0	4.5	5.0	5.5	6.0	6.5
Pure 2.6	-20	PROBE	1.0	0.90	0.75	0.70	0.65	0.55	0.50	0.46	0.44	0.42	0.40
		TIME	0	33.2	86.3	132.3	211.4	307.9	368.2	463.5	606.1	724.9	945.3
	-40	PROBE	3.1	2.8	2.5	2.2	2.0	1.8	1.6	1.4	1.2	1.2	1.0
		TIME	0	11.5	24.5	38.9	54.8	71.9	89.2	112.2	126.6	143.9	177.5
	-60	PROBE	4.2	4.0	3.8	3.6	3.4	3.2	3.0	2.6	2.4	2.3	2.3
		TIME	0	11.5	21.6	31.7	40.4	49.0	60.6	70.5	82.0	96.4	107.9
0.222 % N_2 2.6	-20	PROBE	1.0	0.85	0.75	0.70	0.65	0.60	0.56	0.48	0.44	0.42	-
		TIME	0	34.6	90.6	136.7	203.6	288.1	360.4	491.6	586.6	705.5	-
	-40	PROBE	3.1	2.8	2.5	2.2	2.0	1.8	1.6	1.4	1.2	1.2	1.0
		TIME	0	11.5	26.0	40.4	54.8	67.6	84.9	107.9	125.2	148.2	179.0
1.0	-20	PROBE	1.25	1.15	0.95	0.85	0.75	0.70	0.60	0.60	0.55	0.50	0.45
		TIME	0	20.2	43.3	69.2	93.5	122.3	156.8	193.9	230.1	278.4	314.5
	-40	PROBE	3.1	3.0	2.8	2.6	2.4	2.2	2.0	1.8	1.8	1.6	1.5
		TIME	0	13.0	23.1	34.6	43.3	54.8	63.5	76.2	87.7	99.3	110.8
	-60	PROBE	4.4	4.0	4.0	3.9	3.8	3.6	3.6	3.4	3.4	3.3	3.2
		TIME	0	8.7	14.4	24.5	31.7	40.4	46.1	53.4	60.6	67.8	76.2

Argon - Proforce

Start trig - 1.5 m

Press (torr)	Volt (KV)	Item	z (meters) → 1.5	2.0	2.5	3.0	3.5	4.0	4.5	5.0	5.5	6.0	6.5
0.3	-20	PROBE	-	1.5	1.4	1.35	1.20	1.20	1.10	0.90	0.95	0.90	0.90
		TIME	-	0	14.4	31.7	44.7	63.2	80.5	92.0	106.4	126.6	143.8
	-40	PROBE	-	3.4	3.0	2.9	2.8	2.7	3.0	2.9	2.8	2.7	2.7
		TIME	-	0	11.5	24.5	30.3	41.8	49.0	56.2	66.1	77.6	86.3
	-60	PROBE	4.8	4.8	4.6	4.8	4.6	4.8	4.8	4.6	4.6	4.6	4.6
		TIME	0	10.1	18.8	27.4	36.1	46.1	50.5	46.2	63.5	71.9	80.5

Argon - Antiforce

Press (torr)	Volt (KV)	Item	z (meters) → 1.5	2.0	2.5	3.0	3.5	4.0	4.5	5.0	5.5	6.0	6.5
100	+40	PROBE	3.1	3.0	2.9	2.7	2.7	2.6	2.5	2.4	2.4	2.3	2.2
		TIME		86.4	190.1	298.6	406.0	513.0	643.7	762.5	943.5	1082.9	1278.0
	+60	PROBE	4.6	4.4	4.2	4.2	4.2	4.0	3.9	3.8	3.8	3.6	3.6
		TIME		40.3	83.5	129.6	182.1	236.4	290.7	351.0	398.8	470.1	529.5
	+80	PROBE	6.0	5.8	5.7	5.5	5.4	5.3	5.1	5.0	4.9	4.8	4.7
		TIME		24.5	51.9	82.0	113.6	148.2	182.7	212.8	249.0	298.2	333.4
30	+20	PROBE	1.25	1.2	1.15	1.15	1.1	1.1	1.1	1.1	1.1	-	-
		TIME		180.9	383.7	597.6	822.1	1072.9	1295.9	1574.5	1853.2	-	-
	+40	PROBE	3.2	3.2	3.1	3.0	3.0	2.9	2.8	2.8	2.7	2.6	2.5
		TIME		31.7	70.4	105.0	145.8	195.0	237.2	279.4	327.7	381.9	411.6
	+60	PROBE	4.8	4.7	4.6	4.5	4.4	4.3	4.2	4.1	4.0	3.9	3.8
		TIME		17.3	34.6	51.9	70.5	90.6	107.9	128.0	151.1	174.1	200.2
10	+20	PROBE	1.1	0.9	0.8	0.75	0.70	0.65	0.65	0.6	0.55	0.50	0.5
		TIME		83.5	195.8	322.5	459.3	661.3	809.9	1005.0	1283.7	1562.4	1952.6
	+40	PROBE	3.2	3.0	2.8	2.6	2.4	2.2	2.0	1.8	1.6	1.8	1.6
		TIME		20.2	43.3	64.7	87.7	116.5	145.3	176.4	206.5	242.7	278.9
	+60	PROBE	4.9	4.8	4.8	4.8	4.7	4.6	4.4	4.3	4.2	4.0	4.4
		TIME		14.4	28.8	41.8	56.2	73.3	87.7	102.1	119.4	136.7	148.7

Argon - Antiforce

Press (torr)	Volt (KV)	Item	z (meters) → 1.5	2.0	2.5	3.0	3.5	4.0	4.5	5.0	5.5	6.0	6.5
2.6	+20	PROBE	1.1	1.0	0.9	0.8	0.75	0.65	0.6	0.55	0.55	0.5	0.45
		TIME		34.6	64.7	107.9	155.4	215.7	276.0	348.4	432.8	491.6	562.9
	+60	PROBE	4.8	4.8	4.6	4.5	4.3	4.2	4.0	3.8	3.4	3.8	3.8
		TIME		11.5	20.2	28.8	38.9	47.6	57.7	66.3	73.3	84.9	93.5
0.222% N_2 2.6	+20	PROBE	1.1	1.0	0.9	0.8	0.75	0.65	0.6	0.60	0.55	0.5	0.5
		TIME		33.2	66.1	103.5	153.9	202.2	262.5	334.9	383.2	466.4	549.6
	+40	PROBE	3.4	3.2	2.9	2.7	2.6	2.4	2.2	2.0	1.8	1.6	1.4
		TIME		11.5	26.0	34.6	49.0	62.0	76.2	90.6	105.0	128.0	145.3
1.0	+20	PROBE	1.4	1.25	1.15	1.1	1.0	0.95	0.9	0.85	0.80	0.75	0.7
		TIME		20.2	44.7	69.0	92.0	118.0	143.9	172.7	210.8	247.0	283.2
	+40	PROBE	3.4	3.3	3.2	3.1	2.9	2.8	2.6	2.4	2.2	2.1	2.0
		TIME		11.5	24.5	37.5	49.0	60.6	73.3	84.9	96.4	110.8	125.2
	+60	PROBE	5.2	5.2	5.0	4.8	4.8	4.8	4.6	4.6	4.6	4.4	4.4
		TIME		8.7	18.8	28.8	37.5	46.1	54.8	63.5	73.3	84.9	96.4

Argon - Antiforce

Press (torr)	Volt (KV)	Item	z (meters) → 1.5	2.0	2.5	3.0	3.5	4.0	4.5	5.0	5.5	6.0	6.5
0.3	+20	PROBE	1.5	1.45	1.35	1.3	1.3	1.25	1.2	1.15	1.1	1.1	1.1
		TIME		37.5	67.6	105.0	136.6	173.7	209.9	246.1	276.3	18.5	360.7
	+40	PROBE	3.5	3.3	3.3	3.3	3.3	3.2	3.1	3.1	3.1	3.1	3.0
		TIME		26.0	40.4	82.0	105.0	133.8	153.9	182.7	212.8	236.9	327.4
	+60	PROBE	5.5	5.2	4.8	5.0	4.9	5.0	4.9	4.8	4.8	4.7	4.4
		TIME		23.1	44.7	71.9	94.9	117.9	141.0	164.0	190.1	-	-
0.1	+20	PROBE	1.6	1.6	1.6	1.6	1.6	1.6	1.6	1.6	1.6	1.6	1.6
		TIME		92.1	189.8	298.4	276.1	459.3	542.5	625.7	720.7	837.8	921.4
	+40	PROBE	3.5	3.5	3.5	3.5	3.5	3.5	3.5	3.5	3.5	3.5	3.5
		TIME		86.4	177.5	280.0	358.1	441.3	512.6	607.7	690.8	797.8	899.3
	+60	PROBE	5.0	5.2	5.2	5.2	5.2	5.1	4.8	5.0	4.8	4.8	4.8
		TIME		80.6	158.6	230.9	309.3	351.6	434.8	494.2	553.6	636.8	696.2

APPENDIX C

COMPUTER PROGRAM FOR WAVE SPEED ANALYSIS

The computer program for the analysis of the wave speed raw data is presented in this appendix. The program was written in "BASIC" language for operation by an ASR-33 remote teletype in conjunction with the IBM-370-158 (ITF) computer. The program was written by Dr. William C. Paske.

WAVE SPEED SAMPLE DATA RUN

```
ENTER THE NUMBER OF TAC SCALES USED
  ?   5
ENTER THE TAC RANGE USED (IN NSEC) AND THE NUMBER
OF DATA POINTS IN THIS DATA RANGE
  ?   100,2
ENTER THE DATA POINTS, P(Z)
  ?   4.2
  ?   5.9
ENTER THE TAC RANGE USED (IN NSEC) AND THE NUMBER
OF DATA POINTS IN THIS DATA RANGE
  ?   200,2
ENTER THE DATA POINTS, P(Z)
  ?   4.4
  ?   5.8
ENTER THE TAC RANGE USED (IN NSEC) AND THE NUMBER
OF DATA POINTS IN THIS DATA RANGE
  ?   400,2
ENTER THE DATA POINTS, P(Z)
  ?   4.4
  ?   6.0
ENTER THE TAC RANGE USED (IN NSEC) AND THE NUMBER
OF DATA POINTS IN THIS DATA RANGE
  ?   800,2
ENTER THE DATA POINTS, P(Z)
  ?   4.8
  ?   6.8
ENTER THE TAC RANGE USED (IN NSEC) AND THE NUMBER
OF DATA POINTS IN THIS DATA RANGE
  ?   2000,1
ENTER THE DATA POINTS, P(Z)
  ?   4.6
```

THE RAW TIMES ARE	+/- STD
57.6040	2.2754
82.1180	3.2437
122.2759	6.6640
162.5819	8.8607
246.2838	8.7677
342.7798	12.2030
546.3057	11.7456
783.9458	16.8548
1227.2532	19.0224

NORMALIZED TIMES; T(1)	DELTA TIMES T(N-1)-T(N-2)
24.5140	24.5140
64.6720	40.1580
104.9780	40.3060
188.6798	83.7019
285.1758	96.4960
488.7017	203.5259
726.3418	237.6401
1169.6492	443.3074

THE LINEAR LEAST SQUARES FIT PARAMETERS ARE AS FOLLOWS
THE INTERCEPT IS 9.4702; THE SLOPE IS 0.3583
THE DEVIATION IS ********; THE STANDARD ERROR IS 15.8944

V(0)	BETA	T(0)
4.3532	61.25E-04	11.0752

Z(I)	V(I)
0.0	4.3532
50.0	3.2048
100.0	2.3594
150.0	1.7370
200.0	1.2787
250.0	0.9414
300.0	0.6931
350.0	0.5102
400.0	0.3756
450.0	0.2765

THE EFFECTIVE LENGTH IS 58.502 CM
EFFECTIVE LENGTH VELOCITIES ARE AS FOLLOWS

Z(I)	V(I)
150.0	2.386
200.0	1.457
250.0	1.451
300.0	0.699
350.0	0.606
400.0	0.287
450.0	0.246
500.0	0.132

```
00010 REM R P SCOTT 3/10/75
00015 REM TIMING CALIBRATION
00016 PRINT"ENTER THE NUMBER OF TAC SCALES USED"
00017 INPUT M
00018 FOR J=1 TO M
00020 PRINT"ENTER THE TAC RANGE USED (IN NSEC) AND THE NUMBER"
00025 PRINT"OF DATA POINTS IN THIS DATA RANGE"
00030 INPUT L,N
00032 PRINT"ENTER THE DATA POINTS, P(Z)"
00035 IF L = 50 THEN 50
00040 IF L = 100 THEN 100
00045 IF L = 200 THEN 200
00046 IF L = 400 THEN 400
00047 IF L = 800 THEN 800
00048 IF L = 1000 THEN 1000
00049 IF L = 2000 THEN 2000
00050 FOR I=1 TO N
00060 INPUT T(I,J)
00065 T(I,J)=T(I,J)*6.76+0.781
00066 E(I,J)=T(I,J)*0.0666
00070 NEXT I
00075 GO TO 2050
00100 FOR I=1 TO N
00110 INPUT T(I,J)
00120 T(I,J)=T(I,J)*14.42-2.96
00121 E(I,J)=T(I,J)*0.0395
00130 NEXT I
00140 GO TO 2050
00200 FOR I=1 TO N
00210 INPUT T(I,J)
00220 T(I,J)=T(I,J)*28.79-4.40
00221 E(I,J)=T(I,J)*0.0545
00230 NEXT I
00240 GO TO 2050
00400 FOR I=1 TO N
00410 INPUT T(I,J)
00420 T(I,J)=T(I,J)*60.31-19.08
00421 E(I,J)=T(I,J)*0.0356
00430 NEXT I
00440 GO TO 2050
00800 FOR I=1 TO N
00810 INPUT T(I,J)
00820 T(I,J)=T(I,J)*118.82-24.03
00821 E(I,J)=T(I,J)*0.0215
00830 NEXT I
00840 GO TO 2050
01000 FOR I=1 TO N
01010 INPUT T(I,J)
01020 T(I,J)=T(I,J)*135.64-29.15
01021 E(I,J)=T(I,J)*0.0295
01030 NEXT I
01040 GO TO 2050
02000 FOR I=1 TO N
02010 INPUT T(I,J)
```

```
02020 T(I,J)=T(I,J)*278.69-54.72
02021 E(I,J)=T(I,J)*0.0155
02030 NEXT I
02040 GO TO 2050
02050 NEXT J
02060 PRINT
02070 PRINT"              THE RAW TIMES ARE      +/-    STD"
02500 FOR J=1 TO M
02550 FOR I=1 TO 10
02560 IF T(I,J)=0 THEN 3000
02575 PRINT USING 2580,T(I,J),E(I,J)
02580 :                    ####.####           ##.####
03000 NEXT I
03100 NEXT J
03200 REM TIME NORMALIZATION TO T(1)
03201 PRINT
03202 PRINT"  NORMALIZED TIMES; T(1)      DELTA TIMES T(N-1)-T(N-2)
03205 A=T(1,1)
03210 FOR J=1 TO M
03220 FOR I=1 TO 10
03230 IF T(I,J)=0 THEN 3270
03250 T(I,J)=T(I,J)-A
03270 NEXT I
03280 NEXT J
03290 REM DELTA TIME CALCULATION
03295 B=0
03300 FOR J=1 TO M
03310 FOR I=1 TO 10
03320 IF T(I,J)=0 THEN 3370
03330 D(I,J)=T(I,J)+B
03340 PRINT USING 3350,T(I,J),D(I,J)
03350 :        ####.####                                  ####.####
03360 B=-T(I,J)
03370 NEXT I
03380 NEXT J
03395 REM LINEAR LEAST SQUARES FIT, DELTA T VS NORM. T
03400 S=0
03405 H=0
03410 R=0
03420 V=0
03430 U=0
03440 P=0
03450 FOR J=1 TO M
03460 FOR I=1 TO 10
03470 IF T(I,J)=0 THEN 3540
03480 IF D(I,J)=0 THEN 3540
03490 P=P+1
03500 S=T(I,J)+S
03510 U=T(I,J)*T(I,J)+U
03520 R=D(I,J)+R
03530 V=D(I,J)*T(I,J)+V
03535 H=D(I,J)*D(I,J)+H
03540 NEXT I
```

```
03550 NEXT J
03560 F=((S*V)-(R*U))/((S*S)-(P*U))
03570 G=(R-P*F)/S
03580 REM F= INTERCEPT; G= SLOPE
03590 REM DEVIATION W, AND STANDARD ERROR Z DETERMINATION
03610 W=H-(F*R+G*V)
03620 Z=SQR(W/P)
03672 PRINT
03675 PRINT"THE LINEAR LEAST SQUARES FIT PARAMETERS ARE AS FOLLOWS"
03680 PRINT USING 3700,F,G
03690 PRINT USING 3710,W,Z
03700 :THE INTERCEPT IS ###.####;  THE SLOPE IS ###.####
03710 :THE DEVIATION IS ###.####;  THE STANDARD ERROR IS ###.####
03720 PRINT
03730 PRINT
03750 REM DETERMINATION OF BETA
03760 B=LOG(1+G)/50.
03770 REM DETERMINATION OF T(0)
03780 C=(T(2,1)-F)/(1+G)
03790 REM DETERMINATION OF V(0)
03800 O=(1/B)*G/(G*C+F)
03807 PRINT"    V(0)           BETA        T(0)"
03809 PRINT USING 4000,O,B,C
03810 REM CALCULATE V(I) VS Z(I)
03815 PRINT"            Z(I)           V(I)"
03830 FOR I=1 TO 10
03835 Q=(I-1)*50
03840 X=O*EXP(-B*Q)
03850 PRINT USING 4100,Q,X
03860 NEXT I
04000 :####.####      ##.##!!!!      ####.####
04100 :         ###.#         ###.####
04110 PRINT
04120 PRINT
04121 REM CALCULATION OF EFFECTIVE LENGTH
04122 L1=(EXP(B*50.)-1)/B
04125 PRINT USING 4134,L1
04130 PRINT"EFFECTIVE LENGTH VELOCITIES ARE AS FOLLOWS"
04132 PRINT"       Z(I)                  V(I)"
04133 Q1=100.
04134 :THE EFFECTIVE LENGTH IS ####.### CM
04135 FOR J=1 TO M
04140 FOR I=1 TO 10
04145 IF D(I,J)=0 THEN 4175
04150 O=L1/D(I,J)
04155 Q1=Q1+50
04160 PRINT USING 4170,Q1,O
04170 :       ###.#           ####.###
04175 NEXT I
04180 NEXT J
04190 PRINT
04200 PRINT
04300 PRINT
05000 END
```